Brief sleep disruption alters synaptic structures among hippocampal and neocortical somatostatin-expressing interneurons

Abbreviated title: Sleep loss and interneuron synaptic structure

Authors and affiliations: Frank Raven[1], Alexis Vega Medina[1], Kailynn Schmidt[2], Annie He[1], Anna A. Vankampen[1], Vinodh Balendran[1], Sara J. Aton[1*]

[1] Department of Molecular, Cellular, and Developmental Biology, University of Michigan, Ann Arbor, MI 48019

[2] University of New England College of Osteopathic Medicine, Biddeford, ME 04005

[*] **Corresponding author email:** saton@umich.edu

Number of pages: 20

Number of figures: 5 main, 2 extended

Number of words in Abstract, Introduction, and Discussion: 246, 607, 1,188

Conflict of interest statement: The authors declare no competing financial interests.

Acknowledgements: Figures summarizing results was created using BioRender. This work was supported by NIH research grants R01NS118440 and R01MH135565 and a Chan Zuckerberg Initiative Collaborative Pairs Grant to S.J.A.

Financial Disclosure: The authors have no financial conflicts of interest.

Non-Financial Disclosure: The authors have no non-financial conflicts of interest.

Abstract

Study objectives: Brief sleep loss alters cognition and synaptic structures of principal neurons in hippocampus and neocortex. However, while *in vivo* recording and bioinformatic data suggest that inhibitory interneurons are more strongly affected by sleep loss, it is unclear how sleep and sleep deprivation affect interneurons' synapses. Disruption of the SST+ interneuron population seems to be a critical early sign of neuropathology in Alzheimer's dementia, schizophrenia, and bipolar disorder - and the risk of developing all three is increased by habitual sleep loss. We aimed to test how the synaptic structures of SST+ interneurons in various brain regions are affected by brief sleep disruption.

Methods: We used Brainbow 3.0 to label SST+ interneurons in the dorsal hippocampus, prefrontal cortex, and visual cortex of male *SST-CRE* transgenic mice, then compared synaptic structures in labeled neurons after a 6-h period of *ad lib* sleep, or gentle handling sleep deprivation (SD) starting at lights on.

Results: Dendritic spine density among SST+ interneurons in both hippocampus and neocortex was altered in a subregion-specific manner, with increased overall and thin spine density in CA1, dramatic increases in spine volume and surface area in CA3, and small but significant decreases in spine size in CA1, PFC and V1.

Conclusions: Our suggest that the synaptic connectivity of SST+ interneurons is significantly altered in a brain region-specific manner by a few hours of sleep loss. This suggests a cell type-specific mechanism by which sleep loss disrupts cognition and alters excitatory-inhibitory balance in brain networks.

Significance Statement

Changes to the function of somatostatin-expressing (SST+) interneurons have been implicated in the etiology of psychiatric and neurological disorders in which both cognition and sleep behavior are affected. Here, we measure the effects of very brief experimental sleep deprivation on synaptic structures of SST+ interneurons in hippocampus and neocortex, in brain structures critical for sleep-dependent memory processing. We find that only six hours of sleep deprivation restructures SST+ interneurons' dendritic spines, causing widespread and subregion-specific changes to spine density and spine size. These changes have the potential to dramatically alter excitatory-inhibitory balance across these brain networks, leading to cognitive disruptions commonly associated with sleep loss.

Introduction

Sleep and sleep loss profoundly influence mental health and cognition. As little as a few hours of sleep disruption can alter cognitive performance in both human subjects and animal models [1-5]. Recent studies have implicated disrupted viability and function of somatostatin-expressing (SST+) interneurons in the early stages of neuropathology driving psychiatric and neurological disorders - including Alzheimer's disease [6-10], bipolar disorder, and schizophrenia [11-14]. In all these disorders, sleep seems to be disrupted prior to alterations to cognition and behavior [11-16].

We and others have recently shown that in mice, short-duration experimental sleep deprivation (SD) in the first few hours following learning experiences can impair both hippocampus-dependent memory processing [17-24] and neocortex-dependent memory and synaptic plasticity [25-31]. How does sleep disruption interfere with these processes, and how might sleep promote them? Recent insights have come from both electrophysiological and biochemical studies of sleep effects on the circuits engaged by information processing, including neocortex and hippocampus. For example, in sensory and motor cortical circuits, post-learning sleep is essential for *de novo* dendritic spine formation [25], activation of cellular pathways involved in Hebbian plasticity [32-34], and adaptive firing response property changes [26-30,35,36].

Numerous studies have suggested that SD may have a particularly disruptive effect on the hippocampal microcircuit [37,38]. Transcriptomic responses of the hippocampus to SD are numerous and diverse[18,39]. Episodic and spatial memories are easily disrupted by brief SD occurring at either the encoding, consolidation, or recall stages[40,41]. Behavioral memory deficits have been linked to hippocampal subregion-specific disruption of synaptic plasticity [22-24,42], principal neuron dendritic spine loss [22,43], and neuronal activity disruption[18,19,44-47].

Much of our understanding of SD effects on brain microcircuitry is based on studies which either used bulk tissue (e.g. transcriptomics or biochemistry), or focused on structure or function of excitatory synapses[22,48]. While much less is known about how inhibitory circuits are affected by SD, recent data suggest that transcriptional and functional responses of inhibitory interneurons to sleep loss can be quite different than those of surrounding principal neurons [18,19,45]. Moreover, inhibitory synaptic activity varies across sleep-wake cycles, decreasing over wake or brief SD, in both the hippocampus and neocortex [49-52]. More recent work has suggested that sleep and wake differentially affects the function of synapses corresponding to specific subtypes of interneurons (e.g., SST+ vs. parvalbumin-expressing (PV+) populations) in the hippocampus, with plasticity of the latter, but not the former, being selectively enhanced after a period of wake [53,54]. Recent work from our lab has demonstrated that SST+ interneurons

in the hippocampus are selectively activated by SD, leading to suppression of surrounding principal neuron activity in hippocampal subregions including the dentate gyrus (DG) [19]. Finally, transcriptomic data from the hippocampus suggests that GABA receptor signaling is dramatically altered by SD in the hours following learning [18,46]. Taken together, these data highlight the fact that SD may disrupt cognitive processes via diverse effects on interneuron populations, which are essential for appropriate memory storage [55].

SST+ interneurons have recently been shown to be essential for optimal hippocampal memory processing [19,56] and neocortical sensory [57] and executive functions [58]. Data from our lab and others suggest that SD-driven changes in the function of neocortical and hippocampal SST+ interneurons may be essential to homeostatic and cognitive responses to sleep loss [19,54,59]. To clarify how SD affects SST+ interneurons in hippocampus and neocortex, we used recently-developed genetic tools [60] to resolve dendritic and synaptic structures in these neurons, and characterized dendritic spine alterations among SST+ populations in different hippocampal and neocortical subregions after a very brief, 6-h interval of SD. Like dendritic spines on principal neurons, available data (e.g. from electron or confocal microscopy with immunohistochemistry) suggest that spines are the major site of synaptic input to SST+ interneurons, and that the majority of the dendritic spines on these interneurons receive glutamatergic synapses [61-63]. Moreover, these spines appear to be as plastic as those observed principal neurons; additional spines are formed on hippocampal SST+ interneurons' dendrites in response to learning [64]. We find that structural alterations are present on SST+ interneurons dendritic spines in every brain region quantified after SD, but the direction, extent, and nature of these changes vary from region to region. The diversity of these changes, and their presence across hippocampus and neocortex, suggests that the inhibitory circuits of the brain are profoundly altered by brief sleep loss. These changes to inhibitory microcircuit elements likely underlie some of the cognitive deficits associated with sleep disruption.

Materials and Methods

Mouse husbandry and housing

SST-CRE (*B6N.Cg-Sst*$^{tm2.1(SST\text{-}cre)Zjh}$; Jackson) transgenic male mice on a C57Bl6/J genetic background were group housed on a 12 h light/12 h dark cycle (lights on 9 AM – 9 PM) and under constant temperature (22 ± 2°C), with *ad libitum* food and water access, in standard transparent filter-top caging. Prior to behavioral experiments (see below) mice were single housed with beneficial enrichment (i.e., multiple forms of

nesting material). SD and sleep monitoring was carried out in each mouse's home cage. All animal husbandry and experimental procedures were approved by the University of Michigan Institutional Animal Care and Use Committee (IACUC).

Surgical procedures for AAV-mediated Brainbow labeling

At age 3-15 months (Sleep: 7.1 ± 4.9 months; SD: 6.9 ± 4.0 months) each mouse was transduced with a cocktail of CRE recombinase-dependent AAV vectors to express Brainbow 3.0 (AAV-EF1a-BbTagBY and AAV-EF1a-BbChT; titers ≥ 1×10^{13} vg/mL; Addgene) [60] under isoflurane anesthesia. 1 µl of the AAV cocktail was delivered stereotaxically per brain region as follows: to transduce DG, CA3 and CA1 of dorsal hippocampus, injections were placed at: A/P -2mm, M/L ±2 mm, D/V -2.5 mm and -1.5 mm. Coordinates for neocortical areas V1 and mPFC were: A/P -3 mm, M/L ±3 mm, D/V -0.5 mm, and A/P +1.5 mm, M/L ±0.5 mm, D/V -3 mm and -2.5 mm, respectively.

Handling and SD procedures

Following 9 days of postoperative recovery, mice were single housed and habituated for 5 days to handling procedures (5 min/day). Each mouse was randomly assigned to either Sleep or SD experimental groups. Behavioral experiments started at the beginning of the light phase, two weeks following transduction with Brainbow AAV vectors. SD animals were sleep deprived in their home cage using gentle handling stimulation method for 6 h, during which they were kept awake by gently tapping and/or shaking the cage, and disturbance of nesting material. The necessity of interventions (to disrupt sleep attempts) were documented over the course of the 6-h period, to confirm increases in sleep pressure over the course of deprivation (**Figure 1C**). Mice allowed *ad lib* sleep were monitored visually in 5-min increments to quantify sleep behavior (i.e. assumption of characteristic sleep postures, with closed eyes and immobility) in the home cage (**Figure 1A-B**). This method of sleep quantification has recently been validated as comparable with polysomnographic sleep measurement [65]. Immediately following the 6-h *ad lib* sleep or SD period, mice were euthanized via an overdose of pentobarbital and were perfused transcardially with ice cold PBS followed by 4% paraformaldehyde for brain tissue harvest.

Tissue processing and immunohistochemistry

Perfused brains were post-fixed for 24 hin 4% paraformaldehyde for 24 h at 4°C, washed with PBS, and sectioned coronally (80 µm thickness) using a vibratome. This section thickness was chosen to maximize the extent of dendrite sampling in the Z-plane, without compromising our ability to resolve dendritic spines (i.e., due to light scatter) [60,66]. Free floating brain sections were blocked overnight at 4°C in PBS

containing 5% normalized goat serum and 1% Triton X-100. Each section was then incubated for 72 h at 4°C in PBS with 5% normal donkey serum, 0.5% Triton X-100 and the following primary antibodies chicken anti-EGFP, rat anti-mTFP1, and guinea pig anti-MK2 (all at 1:1000). Following three 1-h rinses at room temperature in PBS with 1% normal donkey serum and 0.5% Triton X-100, sections were incubated for 72 h at 4°C in PBS with 5% normal donkey serum, 0.5% Triton X-100 and the following secondary antibodies: donkey anti-chicken Alexa633, donkey anti-rat Alexa488, and donkey anti-guinea pig Alexa555 (all 1:1000). After secondary antibody incubation, sections received three 1-h rinses and were coverslipped using ProLong Diamond antifade mountant (ThermoFisher Scientific).

Imaging and 3-dimensional reconstruction of dendritic arbors

Images of Brainbow-labeled neurons were acquired using an SP8 confocal microscope (Leica Microsystems) with a 40x oil-immersion objective lens. Images spanned at least 40 µm in depth, using 0.3 µm acquisition steps. Full Z-stack images (0.189 µm/voxel in the X and Y planes, 0.3 µm Z steps) were exported using LAS X software (Leica Microsystems) and traced using Neurolucida360 (MBF Bioscience). For each transduced brain region and animal, Brainbow-labeled neurons with the most complete dendritic arbors represented within the Z-stack (i.e., with no cropping of dendrites within the X and Y planes, and the most complete sampling across the Z plane) were identified. Of those neurons with fully-imaged dendritic arbors, 4-5 were selected at random within each region for 3D reconstruction. Somas were detected automatically (with detection sensitivity varying between 50-80% depending on the signal contrast and intensity), and dendritic arbors were semi-automatically traced. Neurons were selected for analysis with the aim of limiting truncation of dendritic arbors; where dendrites were truncated at a length ≤ 10 µm, these dendrites were excluded from subsequent analysis. Dendritic spines were automatically detected along the full length of traced dendrites, using the following settings: outer range between 1.5 and 3 µm, a minimum height of 0.4 µm, and detector sensitivity set between 75 and 120 µm. Using Neurolucida 360's preset definitions, spine morphology was classified automatically into one of 4 classes: mushroom, stubby, thin, or filopodium [67,68]. The criteria for assigning spines to a specific class are based on prior work quantifying morphology of principal neurons [69], where spine head diameter/neck diameter ratios, backbone length/head diameter ratios, overall backbone length, and overall head diameter are used for classification. In rare instances, spines could not be classified into any of these 4 classes - these are referred to as "none" in **Figure 1**. These non-classifiable spines were most abundant in the DG hilus, where they may reflect "complex spines" or "thorny excrescences" - morphologically unusual synapses previously characterized within that structure, postsynaptic to mossy fiber terminals [70,71]. Each spine's location along the dendrite was used to calculate overall spine density, and for Sholl analysis of spine

distributions along the dendrite. Within each class of spine, surface area and volume parameters were used for subsequent analysis. Spine surface area was defined as the apparent exterior surface area of the spine (in μm^2). Spine volume was calculated as the number of voxels that make up the spine object multiplied by the volume of a single voxel (in μm^3).

Statistical analyses of morphological data

Experimenters were blinded to animal treatment conditions throughout image analyses. Data analyses and generation of summary figures were carried out using GraphPad Prism10 (v10.2.3). To examine the distribution of the different spine types *within* a region, and how the distribution of spine types differed *between* regions, a nested one-way ANOVA was used, followed by Tukey's multiple comparisons tests. For comparisons of spine densities of SST+ interneurons in each brain region between SD and Sleep mice, a nested t-test was used. For Sholl analyses—testing how spine densities vary by distance from the cell soma—we used a repeated-measures two-way ANOVA with a Geisser-Greenhouse correction, using sleep condition and distance from soma as between factors, and subject as within factor. These tests were followed up by multiple comparisons using Fisher's LSD test, to examine if SD affects spine density at a specific distance from soma, for example. Because dendrite length was variable between neurons, Sholl analysis for each subregion was based on shortest common dendrite length for which measures were available for all reconstructed neurons. Data are presented as mean ± S.E.M. Unpaired Kolmogorov-Smirnov (KS) tests were used to compare the distributions of surface area, volume, spine head diameter, and backbone length of spines between SD and Sleep conditions.

Results

Experimental sleep disruption during the rest phase alters the distribution of dendritic spine morphology in SST+ interneurons.

To characterize changes to the SST+ interneuron network following sleep deprivation (SD), SST-CRE mice were transduced with AAV vectors to express Brainbow 3.0 [60] in a CRE recombinase-dependent manner in prefrontal cortex (PFC), primary visual cortex (V1), and dorsal hippocampal DG, CA3, and CA1. Following postoperative recovery, each mouse was habituated to daily handling for 5 days, and were then randomized into freely-sleeping control (Sleep) and SD conditions. Beginning at lights on, mice were either allowed *ad lib* sleep, or were sleep deprived using gentle handling in their home cage over the next 6 h, after which all mice were perfused for SST+ interneuron imaging and morphological analysis. Sleep

behavior was scored behaviorally in control mice, which spent 60-70% of the first 6 h of the rest phase sleeping (**Figure 1A-B**). SD mice showed the expected increase in sleep pressure across the 6-h period of sleep disruption, as evidenced by the increased frequency of interventions (cage taps, cage shakes, next disturbances) needed to maintain wakefulness as SD continued (**Figure 1C**).

Dendritic arbors of Brainbow-labeled SST+ interneurons (*n* = 4-5 neurons per region, per animal) were traced for semi-automated spine detection along their entire length (**Figure 1D-G**). Within the hippocampus, traced Brainbow-labeled neuronal cell bodies were located in the hilus of DG, in the stratum oriens and radiatum of CA3, and in the stratum oriens of CA1. In neocortical structure (PFC and V1), labeled neurons with cell bodies in layers 2/3 and 5 (including putative Martinotti cells)[72,73] were traced. Reconstructed dendritic arbors of hippocampal SST+ interneurons were far more sparse (particularly in CA1 and CA3) than those traced in neocortical subregions, consistent with previous reports of SST+ interneuron morphology in these regions [74-76]. Detected spine morphologies were categorized as thin, stubby, mushroom, or filopodial – using classification methods derived from analysis of dendritic spines on excitatory neurons [69]. Available data from principal (i.e., glutamateric) neurons suggests that stubby and mushroom spine types represent more mature, stable synapses, while thin spines and filopodia are thought to be plastic and/or transient [67,68]. Across all imaged brain areas, nearly all detected spines on SST+ interneurons' dendrites could be classified into these same morphological categories – suggesting similar overall dendritic spine structure between SST+ interneurons and principal neurons. Furthermore, across all brain regions measured, the relative distribution of spine types were very comparable to the distribution reported for principal neurons [9] – although with generally fewer mushroom spines and a greater proportion of stubby spines [77,78]. A small percentage (1-2%) of identified spines in DG (and almost none of those identified in other brain regions) had morphological features that did not meet definitions for the four categories; these atypical spines, which are categorized as "none" in **Figure 1H**, are consistent with previously-described "complex spines" or "thorny excrescences" in the DG hilus (where SST+ interneurons' cell bodies and dendrites reside) [70,71]. In freely-sleeping control mice, thin spines constituted the majority of spines in CA1 and PFC SST+ interneurons, while stubby spines were the predominant spine type in DG, CA3, and V1 (**Extended Figure 1-1A-E**). SD led to changes in the distribution of the four spine morphologies in hippocampal SST+ interneurons. In both CA1 and DG, SST+ interneurons had a decreased proportion of stubby and mushroom (presumptive mature) spines and a corresponding increase in thin (presumptive plastic) spines after SD. CA3 interneurons showed an increased proportion of stubby spines, with reductions in thin and mushroom spines. Similarly, after SD, the proportion of SST+ interneuron spines with stubby morphology increased in both neocortical areas (PFC and V1), with a corresponding

decrease in the proportion of thin spines (and a relative decrease in mushrooms spines in V1). While filopodia were generally rarer in PFC and V1 in freely-sleeping mice, the relative proportion of filopodia decreased in both neocortical structures after SD. Thus, if we extrapolate putative spine functions based on morphological types characterized in principal neurons [67,68], these data suggest different putative effects of SD on SST+ interneurons' synapses, depending on brain region. Namely, SD seemingly reduces mature and stable spine types among interneurons in CA1 and DG while simultaneously increasing immature and plastic spine types. In contrast, mature and stable spine types are more numerous in CA3 and neocortical structures after SD, at the expense of immature and transient spine types.

SD differentially affects overall SST+ interneuron spine density in hippocampal and neocortical subregions.

Overall spine density and total dendrite length, but not total spine numbers, for SST+ interneurons varied by brain region (spine density: $F_{(4, 23)} = 2.9$, $p = 0.0446$; total dendrite length: $F_{(4, 23)} = 57.41$, $p < 0.0001$; spine numbers: $F_{(4, 23)} = 1.4$, $p = 0.2650$; **Figure 2A-B** and **Extended Figure 2-1**), with dendrites of labeled interneurons in neocortical areas generally longer than those in hippocampus, and the shortest dendrites present in CA1 and DG. Spine numbers on SST+ interneurons appeared to be affected by SD with increases observed after SD on interneurons in CA1 (t = 2.388, df = 9, $p = 0.0407$. This led to significant differences in spine density, with increases in CA1 SST+ interneuron overall spine density (nested t-test; t = 2.473, df = 9, $p = 0.0354$) in SD mice. When densities of distinct spine types were compared separately (**Figure 2D-G**), SD-driven, type-specific changes were evident in CA1 (where thin spine density increased significantly [nested t-test; t = 2.992, df = 9, $p = 0.0152$]). Together these data suggest that SST+ interneurons in hippocampus vs. neocortex have divergent responses to SD, with an apparent increase in synaptic input to CA1 interneurons.

Prior work has suggested that the SST+ interneuron population is selectively diminished in hippocampus and neocortex with aging, and that loss of these interneurons is a hallmark of age-related cognitive decline [7,79]. Because mice used in this study covered a range of ages (which were similar in the Sleep and SD conditions; **Extended Figure 2-2A**), we were interested in whether SD effects on spine density were age-specific. Comparing data from young adult mice (3-5 months of age) with those from older adult mice (10-15 months of age), the same apparent increase in overall spine density was observed

in CA1 with SD (**Extended Figure 2-2B**). There were no apparent age-related changes in overall SST+ interneuron spine density in any of the brain regions sampled.

Because SD is known to alter spine density of CA1 and DG principal neurons at specific distances from their somas [22,43], we next tested whether the effects of SD on SST+ interneurons' spine density were spatially constrained using Sholl analysis (**Extended Figure 2-3**). In hippocampal region CA1, which had the most dramatic changes in SST+ interneurons' total spine density with SD, we found main effects of sleep condition ($F_{(1, 9)} = 7.15$, $p < 0.0255$) and distance from soma ($F_{(3.62, 32.6)} = 7.42$, $p < 0.001$), but no significant interaction effect ($F_{(17, 153)} = 1.23$, $p < 0.2454$). Similar results were found for analysis of CA1 thin spine density (main effect of sleep condition, $F_{(1, 9)} = 8.77$, $p = 0.0159$; main effect of distance from soma, $F_{(3.67, 33)} = 4.52$, $p = 0.0061$; sleep × distance interaction, $F_{(17, 153)} = 1.20$, $p = 0.2705$). While densities of some spine types varied significantly with distance in other brain regions, such as thin and stubby spines in CA1 and CA3, respectively, which gradually increased with distance from soma (CA3 stubby spines main effect of distance from soma: $F_{(3.65, 29.2)} = 3.80$, $p < 0.0153$), there were no interaction effects where SD affected density as a function of distance. From these data we conclude that SD drives spatially uniform changes in spine density, affecting spines across the length of SST+ interneurons' dendrites.

SST+ interneurons' dendritic spine size and shape change after SD in a subregion-specific manner.

Because SD can alter dendritic spine size in principal neurons in both neocortex and hippocampus [48,80], we also compared SST+ interneurons' spine size within each brain region between Sleep and SD mice. Cumulative distributions were created separately for spine surface area and volume, for each morphologically-defined spine subtype and brain region. The most impressive changes in spine size after sleep loss were observed in CA3 interneurons, where the size of all spine types (**Figures 3** and **4**) was increased dramatically after SD. Both surface area (**Figure 3**) and volume (**Figure 4**) for CA3 interneurons' stubby (surface area KS test; D = 0.1402; $p < 0.0001$; volume KS test; D = 0.1563; $p < 0.0001$), mushroom (surface area KS test; D = 0.1119; $p < 0.0001$; volume KS test; D = 0.1303; $p < 0.0001$), and thin spine types increased dramatically after SD (surface area KS test; D = 0.1016; $p < 0.0001$; volume KS test; D = 0.1128; $p < 0.0001$). CA3 interneurons' filopodia, while far fewer in number, also showed significant increases in volume (Kolmogorov-Smirnov test; $p = 0.0268$). Because classification of dendritic spines depends on ratios of spine head diameter, neck diameter, and backbone length [69], we also directly compared distributions of head diameter and backbone length (across all detected spines) after Sleep vs. SD. As

shown in **Figure 5**, spine head diameters among CA3 interneurons were also dramatically larger after SD (KS test; D = 0.1671; $p < 0.0001$), while the backbone length distribution decreased (KS test; D = 0.04413; $p < 0.0001$). Together, these data suggest that SD leads to growth and maturation (and potentially, functional strengthening) of synapses on SST+ interneuron dendrites in CA3.

In contrast with the dramatic increases in spine sizes in CA3 interneurons, more modest, but statistically significant, changes in spine size were observed after SD for interneurons in CA1 and DG. In CA1, SD had the most pronounced effect on the density of thin spines – the most abundant spine type on CA1 SST+ interneurons' dendrites (**Figure 1G**). In contrast with the spine size increases observed in CA3, CA1 thin spines' surface area and volume generally decreased after SD (surface area KS test; D = 0.06139; $p < 0.0001$; volume KS test; D = 0.04352; $p < 0.0001$; **Figures 3K** and **4K**). Stubby spines, the second most abundant type on SST+ interneurons in CA1, also showed small, but significant, decreases in surface area and volume after SD (surface area KS test; D = 0.07236; $p = 0.0170$; volume KS test; D = 0.07301; $p < 0.0162$; **Figures 3F** and **4F**). Because both overall and (more specifically) thin spine density is increased in CA1 after SD, one possibility is that this size distribution change is due to new, less-mature spines being added to SST+ interneurons' dendrites across SD. Consistent with this interpretation, spine head diameter (thought to increase with maturation into mushroom-type spines) decreased in CA1 after SD (KS test; D = 0.07856; $p < 0.0001$), while spine length (which is greater in thin spines and filopodia) increased (KS test; D = 0.05087; $p < 0.0001$) (**Figure 5**).

In DG, the effects of SD on dendritic spine morphology were mixed – with overall decreases in the size of mushroom and thin spines (mushroom surface area KS test; D = 0.7240; $p < 0.0001$; mushroom volume KS test; D = 0.6688; $p < 0.0001$; thin surface area KS test; D = 0.04269; $p < 0.0001$; volume KS test; D = 0.01945; $p = 0.0824$; **Figures 3C+M** and **4C+M**), increases in the size of (more-abundant) stubby spines (surface area KS test; D = 0.1532; $p < 0.0001$; volume KS test; D = 0.09250; $p < 0.0001$; **Figures 3H** and **4H**), and mixed effects on filopodia (surface area KS test; D = 0.08966; $p < 0.0001$; volume KS test; D = 0.06819; $p <0.0001$; **Figures 3R** and **4R**), reflecting an SD-driven narrowing of filopodia size distribution. Because the relative abundance of these spine types changes in DG after SD (**Figure 1**), the size changes we observe may reflect transitions in spines' morphology between types. Overall distributions of spine head diameter (KS test; D = 0.05006; $p = 0.0724$) and backbone length (KS test; D = 0.04447; $p = 0.1459$) were unchanged after SD in DG (**Figure 5**). Taken together, these data suggest that, even among different subregions of the dorsal hippocampal circuit, SD can drive bidirectional changes in spine morphology among SST+

interneurons. They also speak to the dramatic and wide-ranging changes evoked by SD in the hippocampal microcircuit in only a few hours.

Neocortical SST+ interneurons showed the most modest changes to spine size after SD. Changes in PFC, small decreases to mushroom and thin spine surface area were observed (mushroom surface area KS test; D = 0.05752; thin surface area KS test; D = 0.03284; p = 0.0434; **Figure 3D+N**), with no corresponding significant changes to spine volume (**Figure 4**). Statistically significant morphological changes in V1 were constrained to stubby spines, which showed decreases in surface area and volume after SD (surface area KS test; D = 0.05054; $p < 0.0001$; volume KS test; D = 0.05417; $p < 0.0001$; **Figures 3J** and **4J**). In both neocortical structures, these changes were associated with overall increases in spine head diameter (PFC - KS test; D = 0.06737; $p < 0.0001$, and V1 - KS test; D = 0.09627; $p < 0.0001$) and decreases in spine length (PFC - KS test; D = 0.03527; $p < 0.0001$, and V1 - KS test; D = 0.05266; $p < 0.0001$) after SD. Taken together, these data suggest that spine type distribution changes (increases in stubby spines and corresponding decreases in thin spines; shown in **Figure 1**) are the most pronounced effects of SD among neocortical SST+ interneurons.

Discussion:

Our data present a dynamic picture of how relatively brief (i.e., 6-hour) SD reconfigures inhibitory networks across the dorsal hippocampus and neocortex (**Figure 6**). We find that in hippocampus, SST+ interneurons in DG undergo small but significant alterations to dendritic spine morphology (but not density) after SD. At the same time, SD causes a large increase to the size (but not density) of *all* spines on CA3 interneurons' dendrites. Meanwhile, CA1 interneurons' spine density is greatly increased by SD, with a corresponding decrease in spine size. Neocortical SST+ interneurons' structures were also affected by SD, albeit modestly - with some spine types slightly decreased in sizein both PFC and V1.

Critically, recent data suggest that spines on SST+ interneurons have similar properties to those on principal neurons. For example, spines associated with these interneurons appear to receive input from glutamatergic and GABAergic presynaptic partners in proportions similar to that observed in pyramidal neurons, with the majority being glutamatergic [61-63]. Moreover, SST+ interneurons' spines exhibit similar learning-driven plasticity, e.g. *de novo* spine formation [64]. Finally, the distributions of spine types we observe on SST+ interneurons' dendrites (**Figure 1**), and changes in density we observe along the dendrites (**Figure 2-3**), are similar to those described for pyramidal neurons in hippocampus and

neocortex [9,77,78]. Because available data suggest that spine functions are conserved between SST+ interneurons and better-characterized principal neurons, we can make inferences about how SD affects the function of these interneurons, and the likely consequences for the networks they reside in. For example, increases in spine density in CA1 SST+ interneurons is likely linked to increased excitatory input to, and activity in, this population during SD [18,19]. In turn, an increase in SST+ interneuron-mediated inhibition could drive overall suppression of activity in the hippocampal network after SD [17,19,81], and corresponding dendritic spine elimination in surrounding pyramidal neurons [22]

Cortical SST+ interneurons (and in particular, Martinotti cells) have been implicated in regulating non-rapid eye movement (NREM) slow wave activity, a marker of the homeostatic sleep response [59], and a subset of SST+ interneurons in PFC (a population projecting to hypothalamic sleep regulatory centers) are activated by SD to increase sleep preparatory behaviors and NREM sleep time [54]. However, the effects of SD on the cortical SST+ population appear to be mixed, with reports of activity increases or decreases reported for different neocortical structures [54,59]. Here we find that at the level of spine size and shape, SD has similar effects on PFC and V1 SST+ interneurons. In both structures, SD leads to small but significant decreases in spine surface area, volume, and backbone length, and larger increases in spine head diameter (**Figures 3** and **4**). Within V1, there was also a trend for reduced spine density – particularly stubby spine density – after SD. While available data suggests that postsynaptic responses of V1 SST+ interneurons may be robust to visual deprivation[82], one possibility is that the increase in visual experience our mice receive during SD could be driving the structural changes we observe. Visually-driven responses in SST+ interneurons tend to be relatively weak and delayed with respect to other V1 neuron populations [83], which may make this population susceptible to Hebbian synaptic depression (and associated dendritic spine changes [84]) in the context of enriched or extensive visual experience. It is worth noting that the morphological spine type most significantly affected in V1 is stubby spines – a spine type which has been proposed to reflect the retraction of mature (i.e. mushroom) spines as they are eliminated, in the context of synaptic depression [67,85]. Taken together, our data are consistent with synapse elimination in V1, where overall spine density, stubby spine density, and stubby spine size all show a decreasing trend after a brief period of SD. Taken together, the changes we observe in neocortical SST+ interneurons are consistent with the recent finding (in V1 and PFC) that *ad lib* sleep simultaneously increases synaptic inhibition and decreases synaptic excitation in neocortical networks [49]. It is also possible that these subtle, SD-driven changes to the structure (and ultimately, function) of these interneurons is directly responsible for changes in slow wave activity observed in the neocortex during recovery sleep [52,59].

We identified more complex changes to the SST+ interneuron network within the hippocampus after SD. In DG, where we had previously characterized SD-driven selective activation of SST+ interneurons [19], SD had the most minor structural effects – i.e., no changes in dendritic spine density, and a mix of changes to spine size (decreases in thin and mushroom spines, increases in stubby spines). In CA3, spines' sizes increased dramatically, across all types. In CA1, overall spine density (and density of the most abundant spine type in CA1 – thin spines) increased after SD, but spine sizes tended to slightly decrease. One possibility is that with respect to presumptive excitatory input at these dendritic spines, opposing changes in spine size and density (and opposing changes between regions CA1 and CA3) might represent cellular or circuit-level homeostasis, preserving overall input to individual SST+ interneurons, constraining their firing rate, and maintaining the relative excitatory-inhibitory balance of the network.

The precise time course of these changes, and the specific roles of NREM and REM sleep, could only be answered in future studies using *in vivo* imaging of dendritic spines. Such studies would also provide a more precise measurement of dendritic spines – which almost certainly undergo subtle changes in size during tissue fixation. Critically, both NREM and REM sleep have been shown to affect rates of spine formation and elimination in neocortical pyramidal neurons [25,86], and to impact the overall activity of both SST+ and parvalbumin-expressing interneurons [51,52] *in vivo*.

An unanswered question is how these changes interact with other functional and structural changes occurring in the brain across SD, and how these changes, together, affect cognitive processes. Recent data from our laboratory have demonstrated that SD drives selective activation in dorsal hippocampal SST+ interneurons, which suppresses activity in surrounding principal neurons [19]. Converging evidence from cell type-specific translating ribosome affinity purification (TRAP)-seq and spatial transcriptomic studies suggests that modulation of excitatory-inhibitory balance in structures such as DG accompany post-learning SD, which may provide a mechanism for disruption of memory consolidation [18,19,46]. At the same time, SD can reduce pyramidal neurons' dendritic spine density in DG [43] and CA1 [22], and can impair Hebbian plasticity at glutamatergic synapses [22,24]. Together, these data suggest a mechanism by which SD-driven increased network inhibition, decreased principal cell activity, or both lead to suppression of hippocampal network output. This idea is supported by human neuroimaging studies in which hippocampal memory encoding and associated hippocampal network activation are impaired after a night of SD [81]. Whether these effects are entirely driven by plastic changes in SST+ interneurons is unclear. However, it is worth noting that SST+ interneurons play a critical role in gating excitatory drive to CA1 pyramidal cells from different input pathways [87], and the information encoding capabilities of DG

granule cells [56,88]. They also directly encode information about space and context essential for hippocampal memory, via plastic changes to their excitatory synapses [71,89-91]. Thus, insofar as the structural changes we observe in hippocampal SST+ interneurons are likely to: 1) outlast the period of SD itself, and 2) disrupt or alter subsequent learning- or recall-driven synaptic interactions or activities in the SST+ population, it is plausible that these changes directly interfere with hippocampal memory processing.

One of the more interesting findings from this study is the difference in SD effects on the SST+ populations in hippocampus vs. neocortex, with the hippocampal SST+ interneuron network undergoing dramatic changes, and neocortical interneurons being only modestly affected. This is surprising, given the reported roles of SST+ interneurons in regulation of sleep propensity and NREM slow wave activity [54,59]. Future studies will be needed to determine how experience in wake (and across SD) contributes to these interneurons' function, and their role in regulating principal neurons' activity [92].

Sleep loss is a growing health concern, affecting millions of people worldwide across all ages, and severely impacting cognitive functioning. The data presented here highlight the diverse and, in some cases, dramatic changes to SST+ interneurons' structure that a few hours of sleep loss can cause. Changes to SST+ interneurons' function, and related changes in excitatory-inhibitory balance, have been implicated in the progression of several neurodegenerative and neuropsychiatric disorders, such as Alzheimer's disease, schizophrenia, bipolar disorder, and major depressive disorder [6-14,93,94]. Understanding the mechanisms through which sleep loss alters the morphology, connectivity, and function of this interneuron population will have wide implications for treating cognitive disruption in these disorders – where alterations in sleep are a common feature.

Author contributions

F.R. and S.J.A. conceived and designed the study. F.R., A.V.M., K.S., A.H., A.A.V., V.B., and S.J.A. performed the research. F.R., A.V.M., K.S., A.H., A.A.V., and S.J.A. analyzed the data. F.R. and S.J.A. interpreted the results and wrote the manuscript. S.J.A. supervised the study.

Figure legends:

Figure 1. A brief period of SD alters dendritic spine morphology distributions in hippocampal and neocortical SST+ interneurons. Brainbow AAV-transduced SST-CRE mice were sleep-deprived for 6 h via gentle handling (*n* = 6), or were allowed to sleep freely in their home cage (*n* = 7), starting at lights on. ***A-B -*** Control mice slept for more than 60-70% of the first half of the light phase, with an average sleep bout length of approximately 50 min. ***C –*** Gentle handling interventions needed to prevent sleep in SD mice (cage taps, cage shakes, and nest disturbances) increased over the course of the 6-h SD experiment. ***D-G -***Representative images across the z-axis (**D**), maximum intensity projection images (***E***) showing Brainbow-labeled SST+ interneurons in each of the examined brain regions, corresponding traced neuronal dendritic arbors (***F***), and detail of inset, highlighting dendritic spines (***G***). Scale bars indicate 100 µm. ***H -*** Distribution of spine subtypes for quantified for neurons in each region in freely-sleeping and SD mice. Supporting data in **Extended Figure 1-1**.

Extended Figure 1-1. Spine type distribution on SST+ interneurons differs with brain region in freely-sleeping mice. *Supports **Figure 1**. **A -*** Thin spines had the highest density in hippocampal CA1. ***B-D -*** In CA3, DG, and PFC, stubby and thin spines had the highest density. ***E -*** In V1, stubby spines had the highest density. *n* = 24-30 neurons/region.

Figure 2. SD differentially affects SST+ interneurons' spine density in hippocampal and neocortical subregions. ***A-C -*** SD significantly increased total spine density in hippocampal CA1, but did not significantly affect spine density in SST+ interneurons sampled from other brain regions. ***D-G -*** Spine density in each region by type. Thin spine density (***F***) was increased in CA1 after SD. Data points are shown for *n* = 24-30 total neurons/region/condition, with 4-5 neurons/region/animal. * indicates $p < 0.05$, nested t-test. Supporting data in **Extended Figure 2-1, 2-2, and 2-3**.

Extended Figure 2-1. Spine densities of specific spine subtypes differ between brain regions. *Supports **Figure 2**. **A-B -*** spine density, but not spine numbers, differed between brain regions, with higher densities observed in the hippocampal areas compared to neocortical areas. ***C-F -*** Thin spine and filopodia densities differed between brain regions, while densities of mushroom and stubby spines were comparable

between regions. n = 24-30 neurons/region. * $p < 0.05$, ** $p < 0.01$, *** $p < 0.001$, **** $p < 0.0001$, Tukey's multiple comparisons test.

Extended Figure 2-2. Mouse age does not interact with the effects of sleep deprivation on SST+ interneuron's spine densities. *Supports* ***Figure 2***. ***A*** **-** Age range does not differ between the two experimental groups, but two clusters of mouse ages were present in both Sleep and SD mice: young adult (3-5 months old) and older adult (10-15 months old). ***B*** **-** Data split for age groups 3-5 months old and 10-15 months old. SST+ cell's spine density was comparable across age and condition for all examined brain regions.

Extended Figure 2-2. SD affects spine density uniformly along dendrites. *Supports* ***Figure 2***. Sholl analysis of spine densities of specific morphological subtypes at specific distances from the cell soma. ***A-E*** **-** SD increased overall spine density along the whole dendrite among CA1 interneurons. ***F-O*** **-** Mushroom and stubby spine densities showed no sleep condition × distance interaction. ***P-T*** **-** Thin spine densities increased uniformly along CA1 SST+ interneurons' dendrites after SD. ***U-Y*** **-** Filopodia was unaffected by SD. * and ** indicate $p < 0.05$ and $p < 0.01$, Fisher's LSD *post hoc* test.

Figure 3. SD alters SST+ interneuron spines' surface area in a subregion-specific manner. ***A-E*** **-** SD increased mushroom spines' surface area in CA3, and simultaneously decreased their surface area in DG and PFC. ***F-J*** **-** The surface area of stubby spines was altered by SD in CA1, CA3, DG, and V1, with dramatic increases in CA3. ***K-O*** **-** SD increased the surface area of thin spines in CA1 and CA3, and decreased their surface area in DG and PFC. ***P-T*** **-** The surface area of filopodia were not affected by SD for any region except for DG.

Figure 4. SD alters SST+ interneuron spines' volume in a subregion-specific manner. ***A-E*** **-** SD increased mushroom spines' volume in CA3, and simultaneously decreased their volume in DG – mirroring changes in surface area. ***F-J*** **-** Stubby spine volumes were altered by SD in all regions except PFC, with dramatic increases in CA3. ***K-O*** **-** SD increased the volume of CA3 thin spines, and decreased the volume of CA1 thin

spines. ***P-T –*** SD significantly increased the volume of filopodia in CA3, and modestly affected volume distributions in DG.

Figure 5. SD differentially affects spine head diameter and spine length in specific brain regions. *A-E* - SD increased spine head diameter in the CA1 region of the hippocampus, while it reduced their diameter in hippocampal area CA3 and neocortical area PFC and V1. ***F-J* -** Spine head backbone length was decreased in the CA1 area, but increased areas CA3, PFC, and V1.

Figure 6. Summary of changes to SST+ interneuron structures in neocortex and hippocampus.

Data Availability Statement: All data will be made available to investigators after publication, if requested.

References cited :

1. Abel, T., Havekes, R., Saletin, J.M., and Walker, M.P. (2013). Sleep, plasticity and memory from molecules to whole-brain networks. Curr Biol *23*, R774-788.
2. Born, J., and Wilhelm, I. (2012). System consolidation of memory during sleep. Psychol Res *76*, 192-203.
3. Diekelmann, S., and Born, J. (2010). The memory function of sleep. Nat Rev Neurosci *11*, 114-126.
4. Ellenbogen, J.M., Payne, J.D., and Stickgold, R. (2006). The role of sleep in declarative memory consolidation: passive, permissive, active or none? Current Opinion in Neurobiology Motor systems / Neurobiology of behaviour *16*, 716-722.
5. Puentes-Mestril, C., Roach, J., Niethard, N., Zochowski, M., and Aton, S.J. (2019). How rhythms of the sleeping brain tune memory and synaptic plasticity. Sleep *42*, pii: zsz095. 10.1093/sleep/zsz095.
6. Gabitto, M., Travaglini, K., and Rachleff, V. (2024). Integrated multimodal cell atlas of Alzheimer's disease. Nat Neurosci. 10.1038/s41593-024-01774-5.
7. Mathys, H., Peng, Z., Boix, C., Victor, M., Leary, N., S, B., Abdelhady, G., Jiang, X., Ng, A., Ghafari, K., et al. (2023). Single-cell atlas reveals correlates of high cognitive function, dementia, and resilience to Alzheimer's disease pathology. Cell *186*, 4365-4385.
8. Gazestani, V., Kamath, T., Nadaf, N., Dougalis, A., Burris, S., Rooney, B., Junkkari, A., Vanderburg, C., Pelkonen, A., Gomez-Budia, M., et al. (2023). Early Alzheimer's disease pathology in human cortex involves transient cell states. Cell *186*, 4438-4453.
9. Guptarak, J., Scaduto, P., Tumurbaatar, B., Zhang, W., Jupiter, D., Taglialatela, G., and Fracassi, A. (2024). Cognitive integrity in Non-Demented Individuals with Alzheimer's Neuropathology is associated with preservation and remodeling of dendritic spines. Alzheimers Dement *20*, 4677-4691.
10. Lauterborn, J., Scaduto, P., Cox, C., Schulmann, A., Lynch, G., Gall, C.M., Keene, C., and Limon, A. (2021). Increased excitatory to inhibitory synaptic ratio in parietal cortex samples from individuals with Alzheimer's disease Nat Commun *12*, 2603.
11. Konradi, C., Yang, C.K., Zimmerman, E.I., Lohmann, K.M., Gresch, P., Pantazopoulos, H., Berretta, S., and Heckers, S. (2011). Hippocampal interneurons are abnormal in schizophrenia Schizophr Res *131*, 165-173.
12. Wang, A., Lohmann, K.M., Yang, C., Zimmerman, E.I., Pantazopoulos, H., Herring, N., Berretta, S., Heckers, S., and Konradi, C. (2011). Bipolar disorder type 1 and schizophrenia are accompanied by decreased density of parvalbumin- and somatostatin-positive interneurons in the parahippocampal region. . Acta Neuropathol *122*, 615-626.
13. Dienel, S., Dowling, K., Barile, Z., Bazmi, H., Liu, A., Vespoli, J., Fish, K., and Lewis, D.A. (2023). Diagnostic Specificity and Association With Cognition of Molecular Alterations in Prefrontal Somatostatin Neurons in Schizophrenia. JAMA Psychiatry *80*, 1235-1245.
14. Dienel, S.J., and Lewis, D.A. (2019). Alterations in cortical interneurons and cognitive function in schizophrenia Neurobiol Dis *131*.
15. Wamsley, E.J., Tucker, M.A., Shinn, A.K., Ono, K.E., McKinley, S.K., Ely, A.V., Goff, D.C., Stickgold, R., and Manoach, D.S. (2012). Reduced sleep spindles and spindle coherence in schizophrenia: mechanisms of impaired memory consolidation? . Biol Psychiatry *71*, 154-161.
16. Zhang, Y., Quinones, G.M., and Ferrarelli, F. (2020). Sleep spindle and slow wave abnormalities in schizophrenia and other psychotic disorders: Recent findings and future directions Schizophr Res *221*, 29-36.

17. Ognjanovski, N., Broussard, C., Zochowski, M., and Aton, S.J. (2018). Hippocampal Network Oscillations Rescue Memory Consolidation Deficits Caused by Sleep Loss. Cereb. Cortex *28*, 3711-3723. 10.1093/cercor/bhy174.
18. Delorme, J., Wang, L., Kodoth, V., Wang, Y., Ma, J., Jiang, S., and Aton, S.J. (2021). Hippocampal neurons' cytosolic and membrane-bound ribosomal transcript profiles are differentially regulated by learning and subsequent sleep. Proc Natl Acad Sci USA *118*.
19. Delorme, J., Wang, L., Roig Kuhn, F., Kodoth, V., Ma, J., Martinez, J.D., Raven, F., Toth, B.A., Balendran, V., Vega Medina, A., et al. (2021). Sleep loss drives acetylcholine- and somatostatin interneuron-mediated gating of hippocampal activity, to inhibit memory consolidation. Proc Natl Acad Sci USA *118*.
20. Martinez, J.D., Wilson, L.G., Peterson, K.G., Brancaleone, W.P., Popke, D.S., Caicedo Garzon, V., Perez Tramble, R.E., Donnelly, M.J., Torres, D., Mendez Ortega, S.L., et al. (2024). Hypnotic treatment reverses NREM sleep disruption and EEG desynchronization in a mouse model of Fragile X syndrome to rescue memory consolidation deficits. . Cell Rep *43*, 114266.
21. Prince, T.M., Wimmer, M., Choi, J., Havekes, R., Aton, S., and Abel, T. (2014). Sleep deprivation during a specific 3-hour time window post-training impairs hippocampal synaptic plasticity and memory. Neurobiol Learn Mem *109*, 122-130.
22. Havekes, R., Park, A.J., Tudor, J.C., Luczak, V.G., Hansen, R.T., Ferri, S.L., Bruinenberg, V.M., Poplawski, S.G., Day, J.P., Aton, S.J., et al. (2016). Sleep deprivation causes memory deficits by negatively impacting neuronal connectivity in hippocampal area CA1. eLife *5*, pii: e13424.
23. Tudor, J.C., Davis, E.J., Peixoto, L., Wimmer, M.E., van Tilborg, E., Park, A.J., Poplawski, S.G., Chung, C.W., Havekes, R., Huang, J., et al. (2016). Sleep deprivation impairs memory by attenuating mTORC1-dependent protein synthesis. Sci Signal *9*, ra41.
24. Vecsey, C.G., Baillie, G.S., Jaganath, D., Havekes, R., Daniels, A., Wimmer, M., Huang, T., Brown, K.M., Li, X.Y., Descalzi, G., et al. (2009). Sleep deprivation impairs cAMP signalling in the hippocampus. Nature *461*, 1122-1125.
25. Yang, G., Lai, C.S., Cichon, J., Ma, L., Li, W., and Gan, W.B. (2014). Sleep promotes branch-specific formation of dendritic spines after learning. Science *344*, 1173-1178.
26. Martinez, J.D., Donnelly, M.J., Popke, D.S., Torres, D., Wilson, L.G., Brancaleone, W.P., Sheskey, S., Lin, C.-M., Clawson, B.C., Jiang, S., and Aton, S.J. (2023). Enriched binocular experience followed by sleep optimally restores binocular visual cortical responses in a mouse model of amblyopia. Communications Biology *6*, 408.
27. Aton, S.J., Suresh, A., Broussard, C., and Frank, M.G. (2014). Sleep promotes cortical response potentiation following visual experience. Sleep *37*, 1163-1170.
28. Durkin, J., Suresh, A.K., Colbath, J., Broussard, C., Wu, J., Zochowski, M., and Aton, S.J. (2017). Cortically coordinated NREM thalamocortical oscillations play an essential, instructive role in visual system plasticity. Proceedings National Academy of Sciences *114*, 10485-10490.
29. Clawson, B.C., Durkin, J., Suresh, A.K., Pickup, E.J., Broussard, C.G., and Aton, S.J. (2018). Sleep Promotes, and Sleep Loss Inhibits, Selective Changes in Firing Rate, Response Properties and Functional Connectivity of Primary Visual Cortex Neurons. Frontiers in Systems Neuroscience *12*, 40. doi: 10.3389/fnsys.2018.00040.
30. Durkin, J., and Aton, S.J. (2016). Sleep-Dependent Potentiation in the Visual System Is at Odds with the Synaptic Homeostasis Hypothesis. Sleep *39*, 155-159.
31. Miyamoto, D., Hirai, D., Fung, C.C., Inutsuka, A., Odagawa, M., Suzuki, T., Boehringer, R., Adaikkan, C., Matsubara, C., Matsuki, N., et al. (2016). Top-down cortical input during NREM sleep consolidates perceptual memory. Science *352*, 1315-1318.
32. Aton, S.J., Seibt, J., Dumoulin, M., Jha, S.K., Steinmetz, N., Coleman, T., Naidoo, N., and Frank, M.G. (2009). Mechanisms of sleep-dependent consolidation of cortical plasticity. Neuron *61*, 454-466.

33. Dumoulin, M.C., Aton, S.J., Watson, A.J., Renouard, L., Coleman, T., and Frank, M.G. (2015). Extracellular Signal-Regulated Kinase (ERK) Activity During Sleep Consolidates Cortical Plasticity In Vivo. Cereb. Cortex *25*, 507-515. 10.1093/cercor/bht250.
34. Seibt, J., Dumoulin, M., Aton, S.J., Coleman, T., Watson, A., Naidoo, N., and Frank, M.G. (2012). Protein synthesis during sleep consolidates cortical plasticity in vivo. Curr Biol *22*, 676-682.
35. Aton, S.J., Broussard, C., Dumoulin, M., Seibt, J., Watson, A., Coleman, T., and Frank , M.G. (2013). Visual experience and subsequent sleep induce sequential plastic changes in putative inhibitory and excitatory cortical neurons. Proc Natl Acad Sci U S A *110*, 3101-3106.
36. Clawson, B.C., Pickup, E.J., Enseng, A., Geneseo, L., Shaver, J., Gonzalez-Amoretti, J., Zhao, M., York, A.K., Kuhn, F.R., Swift, K.M., et al. (2021). Causal role for sleep-dependent reactivation of learning-activated sensory ensembles for fear memory consolidation. Nat Communications *12*.
37. Krause, A.J., Simon, E.B., Mander, B.A., Greer, S.M., Saletin, J.M., Goldstein-Piekarski, A.N., and Walker, M.P. (2017). The sleep-deprived human brain. Nat Rev Neurosci *18*, 404-418. doi:10.1038/nrn.2017.55.
38. Prince, T.M., and Abel, T. (2013). The impact of sleep loss on hippocampal function. Learn Mem *20*, 558-569.
39. Y, V., ZJ, P., EN, W., S, C., LC, L., LC, L., T, N.-J., and T., A. (2023). Spatial transcriptomics reveals unique gene expression changes in different brain regions after sleep deprivation. Nat Commun *14*, 7095.
40. Heckman, P.R.A., Roig-Kuhn, F., Meerlo, P., and Havekes, R. (2020). A brief period of sleep deprivation negatively impacts the acquisition, consolidation, and retrieval of object-location memories. Neurobiol Learn Mem *175*.
41. Contatto Rossi, V., Ayako Tiba, P., Di Monteiro Moreira, K., Lima Ferreira, T., Menezes Oliveira, M., and Suchecki, D. (2014). Effects of sleep deprivation on different phases of memory in the rat: dissociation between contextual and tone fear conditioning tasks Front Behav Neurosci *8*.
42. Abel, T., Havekes, R., Salatin, J.M., and Walker, M.P. (2013). Sleep, Plasticity and Memory from Molecules to Whole-Brain Networks. Curr Biol *23*, R774-788.
43. Raven, F., Meerlo, P., Van der Zee, E.A., Abel, T., and Havekes, R. (2019). A brief period of sleep deprivation causes spine loss in the dentate gyrus of mice. Neurobiol Learn Mem *160*, 83-90.
44. Delorme, J.E., Kodoth, V., and Aton, S.J. (2019). Sleep loss disrupts Arc expression in dentate gyrus neurons. Neurobiol Learn Mem *160*, 73-82.
45. Puentes-Mestril, C., Delorme, J., Wang, L., Donnelly, M., Popke, D., Jiang, S., and Aton, S.J. (2021). Sleep loss drives brain region- and cell type-specific alterations in ribosome-associated transcripts involved in synaptic plasticity and cellular timekeeping. J Neurosci *41*, 5386-5398.
46. Wang, L., Park, L., Wu, W., King, D., Vega-Medina, A., Raven, F., Martinez, J., Enseng, A., McDonald, K., Yang, Z., et al. (2024). Sleep-dependent engram reactivation during hippocampal memory consolidation associated with subregion-specific biosynthetic changes. iScience *27*, 109408. 10.1016/j.isci.2024.109408
47. Skilling, Q.M., Eniwaye, B., Clawson, B.C., Shaver, J., Ognjanovski, N., Aton, S.J., and Zochowski, M. (2021). Acetylcholine-gated current translates wake neuronal firing rate information into a spike timing-based code in Non-REM sleep, stabilizing neural network dynamics during memory consolidation PLoS Computational Biology *17*, e1009424.
48. de Vivo, L., Bellesi, M., Marshall, W., Bushong, E.A., Ellisman, H., Tononi, G., and Cirelli, C. (2017). Ultrastructural evidence for synaptic scaling across the wake/sleep cycle. Science *355*, 507-510.
49. Bridi, M.C.D., Zong, F.-J., Min, X., Luo, N., Tran, T., Qiu, J., Severin, D., Zhang, X.-T., Wang, G., Zhu, Z.-J., et al. (2020). Daily Oscillation of the Excitation-Inhibition Balance in Visual Cortical Circuits. Neuron *105*, 621-629.

50. Niethard, N., Burgalossi, A., and Born, J. (2017). Plasticity during Sleep Is Linked to Specific Regulation of Cortical Circuit Activity. Front Neural Circuits *11*, 1-9.
51. Niethard, N., Hasegawa, M., Itokazu, T., Oyanedel, C.N., Born, J., and Sato, T.R. (2016). Sleep-Stage-Specific Regulation of Cortical Excitation and Inhibition. Curr Biol *26*, 2739-2749.
52. Niethard, N., Ngo, H.V., Ehrlich, I., and Born, J. (2018). Cortical Circuit Activity Underlying Sleep Slow Oscillations and Spindles. Proc Natl Acad Sci U S A *115*, E9220-9229. doi: 10.1073/pnas.1805517115.
53. Wu, K., Han, W., and Lu, W. (2022). Sleep and wake cycles dynamically modulate hippocampal inhibitory synaptic plasticity. PLoS Biology *20*, e3001812.
54. Tossell, K., Yu, X., Giannos, P., Anuncibay Soto, B., Nollet, M., Yustos, R., Miracdca, G., Vicente, M., Miao, A., Hsieh, B., et al. (2023). Somatostatin neurons in prefrontal cortex initiate sleep-preparatory behavior and sleep via the preoptic and lateral hypothalamus. Nat Neurosci *26*, 1805-1819.
55. Raven, F., and Aton, S.J. (2021). The Engram's Dark Horse: How Interneurons Regulate State-Dependent Memory Processing and Plasticity. . Front Neural Circuits *15*, 750541.
56. Stefanelli, T., Bertollini, C., Luscher, C., Muller, D., and Mendez, P. (2016). Hippocampal Somatostatin Interneurons Control the Size of Neuronal Memory Ensembles. Neuron *89*, 1074-1085.
57. Zhang, S., Xu, M., Kamigaki, T., Hoang Do, J.P., Chang, W.C., Jenvay, S., Miyamichi, K., Luo, L., and Dan, Y. (2014). Selective attention. Long-range and local circuits for top-down modulation of visual cortex processing. Science *345*, 660-665.
58. Brockway, D., Griffith, K., Aloimonos, C., Clarity, T., Moyer, J., Smith, G., NC, D., Shakhawat Hossain, M., Drew, P., Gordon, J.A., et al. (2023). Somatostatin peptide signaling dampens cortical circuits and promotes exploratory behavior. Cell Rep *42*, 112976.
59. Funk, C.M., Peelman, K., Bellesi, M., Marshall, W., Cirelli, C., and Tononi, G. (2017). Role of Somatostatin-Positive Cortical Interneurons in the Generation of Sleep Slow Waves. J Neurosci *37*, 9132-9148.
60. Cai, D., Cohen, K.B., Luo, T., Lichtman, J.W., and Sanes, J.R. (2013). Improved tools for the Brainbow toolbox. Nature Methods *10*, 540-547.
61. Guirado, R., Perez-Rando, M., Sanchez-Materrodona, D., Castillo-Gomez, E., Liberia, T., Rovira-Esteban, L., Varea, E., Crespo, C., Blasco-Ibanez, J., and Nacher, J. (2013). The Dendritic Spines of Interneurons Are Dynamic Structures Influenced by PSA-NCAM Expression. Cereb Cortex *24*, 3014-3024.
62. Keck, T., Scheuss, V., Jacobsen, R., Wierenga, C., Eysel, U., Bonhoeffer, T., and Hubener, M. (2011). Loss of sensory input causes rapid structural changes of inhibitory neurons in adult mouse visual cortex Neuron *71*, 869-882.
63. Takacs, V., Bardoczi, Z., Orosz, A., Major, A., Tar, L., Berki, P., Papp, P., Mayer, M.I., Sebok, H., Zsolt, L., et al. (2024). Synaptic and dendritic architecture of different types of hippocampal somatostatin interneurons. PLoS Biology *22*, e3002539.
64. Schmid, L.C., Mittag, M., Poll, S., Steffen, J., Wagner, J., Geis, H.-R., Schwarz, I., Schmidt, B., Schwarz, M.K., Remy, S., and Fuhrmann, M. (2016). Dysfunction of Somatostatin-Positive Interneurons Associated With Memory Deficits in an Alzheimer's Disease Model Neuron *92*, 114-125.
65. Martinez, J.D., Brancaleone, W.P., Peterson, K.G., Wilson, L.G., and Aton, S.J. (2023). Atypical hypnotic compound ML297 restores sleep architecture immediately following emotionally valenced learning, to promote memory consolidation and hippocampal network activation during recall Sleep *46*, zsac301.

66. Djurisic, M., Vidal, G., Mann, M., Aharon, A., Kim, T.-K., Ferrao Santos, A., Zuo, Y., Hubener, M., and Shatz, C. (2013). PirB regulates a structural substrate for cortical plasticity. Proc Natl Acad Sci U S A *110*, 20771-20776.
67. Hering, H., and Sheng, M. (2001). Dentritic spines : structure, dynamics and regulation. Nat Rev Neurosci *2*, 880-888.
68. Runge, K., Cardoso, C., and de Chevigny, A. (2020). Dendritic Spine Plasticity: Function and Mechanisms. Front Synaptic Neurosci *12*, 36.
69. Rodriguez, A., Ehlenberger, D., Dickstein, D., Hof, P., and Wearne, S.L. (2008). Automated Three-Dimensional Detection and Shape Classification of Dendritic Spines from Fluorescence Microscopy Images. PLoS One *3*, e1997.
70. Scharfman, H., and Myers, C. (2012). Hilar mossy cells of the dentate gyrus: a historical perspective. Front Neural Circuits *6*, 106.
71. Grigoryan, G., Harada, H., Knobloch-Bollmann, H., Kilias, A., Kaufhold, D., Kulik, A., Eyre, M., and Bartos, M. (2023). Synaptic plasticity at the dentate gyrus granule cell to somatostatin-expressing interneuron synapses supports object location memory. Proc Natl Acad Sci U S A *120*, e2312752120.
72. Naka, A., Veit, J., Shababo, B., Chance, R.K., Risso, D., Stafford, D., Snyder, B., Egladyous, A., Chu, D., Sridhara, S., et al. (2019). Complementary networks of cortical somatostatin interneurons enforce layer specific control Elife *8*.
73. Wang, Y., Toledo-Rodriguez, M., Gupta, A., Wu, C., Siberberg, G., Luo, J., and Markram, H. (2004). Anatomical, physiological and molecular properties of Martinotti cells in the somatosensory cortex of the juvenile rat. J Physiol *561* (*1*), 65-90.
74. Gilabert-Juan, J., Bueno-Fernandez, C., Castillo-Gomez, E., and Nacher, J. (2017). Reduced interneuronal dendritic arborization in CA1 but not in CA3 region of mice subjected to chronic mild stress. Brain Behav *7*, e00534.
75. Veldman, M.B., Park, C.S., Eyermann, C., Zhang, J., Zuniga-Sanchez, E., Hirano, A., Daigle, T., Foster, N., Zhu, M., Fangfelder, P., et al. (2020). Brainwide Genetic Sparse Cell Labeling to Illuminate the Morphology of Neurons and Glia with Cre-Dependent MORF Mice Neuron *108*, 111-127.
76. Scala, F., Kobak, D., Bernabucci, M., Bernaerts, Y., Cadwell, C., Ramon Castro, J., Harmanis, L., Jiang, X., Laturnus, S., Miranda, E., et al. (2021). Phenotypic variation of transcriptomic cell types in mouse motor cortex Nature *598*, 144-150.
77. Celora, L., JAudon, F., Vitale, C., and Cingolani, L. (2023). Regulation of dendritic spine length in corticopontine layer V pyramidal neurons by autism risk gene β3 integrin. Mol Brain *16*, 49.
78. Pchitskaya, E., Vasiliev, P., Smirnova, D., Chukanov, V., and Bezprozvanny, I. (2023). SpineTool is an open-source software for analysis of morphology of dendritic spines. Scientific Reports *13*, 10561.
79. Gabitto, M., Travaglini, J., and Rachleff, V. (2024). Integrated multimodal cell atlas of Alzheimer's disease. Nat Neurosci. https://doi.org/10.1038/s41593-024-01774-5.
80. Spano, G.M., Banningh, S.W., Marshall, W., de Vivo, L., Bellesi, M., Loschky, S.S., Tononi, G., and Cirelli, C. (2019). Sleep Deprivation by Exposure to Novel Objects Increases Synapse Density and Axon-Spine Interface in the Hippocampal CA1 Region of Adolescent Mice. J Neurosci *39*, 6613-6625.
81. Yoo, S.-S., Hu, P.T., Gujar, N., Jolesz, F.A., and Walker, M.P. (2007). A deficit in the ability to form new human memories without sleep. *10*, 385-392.
82. Grier, B., Parkins, S., Omar, J., and Lee, H.-K. (2023). Selective plasticity of fast and slow excitatory synapses on somatostatin interneurons in adult visual cortex. Nat Commun *14*, 7165.

83. Ma, W.-P., Liu, B.-H., Li, Y.-T., Huang, Z.J., Zhang, L., and Tao, H. (2010). Visual Representations by Cortical Somatostatin Inhibitory Neurons—Selective But with Weak and Delayed Responses. J Neurosci *30*, 14371-14379.
84. Zhou, Q., Homma, K., and Poo, M.-M. (2004). Shrinkage of Dendritic Spines Associated with Long-Term Depression of Hippocampal Synapses. Neuron *44*, P749-757.
85. Hasegawa, S., Sakuragi, S., Tominaga-Yoshino, K., and Ogura, A. (2015). Dendritic spine dynamics leading to spine elimination after repeated inductions of LTD. Scientific Reports *5*, 7707.
86. Zhou, Y., Lai, C.S.W., Bai, Y., Li, W., Zhou, R., Yang, G., Frank, M.G., and Gan, W.-B. (2020). REM sleep promotes experience-dependent dendritic spine elimination in the mouse cortex Nat Communications *11*.
87. Leao, R., Mikulovic, S., Leao, K., Mungaba, H., Gezelius, H., Enjin, A., Patra, K., Eriksson, A., Loew, L., Tort, A., and Kullander, K. (2012). OLM interneurons differentially modulate CA3 and entorhinal inputs to hippocampal CA1 neurons. Nat Neurosci *15*, 1524–1530.
88. Raza, S.A., Albrecht, A., Caliskan, G., Muller, B., Demiray, Y.E., Ludewig, S., Meis, S., Faber, N., Hartig, R., Schraven, B., et al. (2017). HIPP neurons in the dentate gyrus mediate the cholinergic modulation of background context memory salience. Nat Communications *8*.
89. Morales, C., Facundo Morici, J., Espinosa, N., Sacson, A., Lara-Vasquez, A., Garcia-Perex, M.A., Bekinschtein, P., Weisstaub, N.V., and Fuentealba, P. (2021). Dentate Gyrus Somatostatin Cells are Required for Contextual Discrimination During Episodic Memory Encoding Cereb Cortex *31*, 1046-1059.
90. Honore, E., and Lacaille, J.C. (2022). Object location learning in mice requires hippocampal somatostatin interneuron activity and is facilitated by mTORC1-mediated long-term potentiation of their excitatory synapses. Mol Brain *15*, 101.
91. Zicho, K., Sos, K.E., Papp, P., Barth, A.M., Misak, E., Mayer, M.I., Sebesteny, R.Z., and Nyiri, G. (2023). Fear memory recall involves hippocampal somatostatin interneurons. PLoS Biology *21*.
92. Havekes, R., and Aton, S.J. (2020). Impacts of Sleep Loss Versus Waking Experience on Brain Plasticity: Parallel or Orthogonal? Trends in Neuroscience *43*, 385-393.
93. Song, Y.-H., Yoon, J., and Lee, S.-H. (2021). The role of neuropeptide somatostatin in the brain and its application in treating neurological disorders. Exp Mol Med *53*, 328-338.
94. Anderson, K., Collins, M., Kong, R., Fang, K., Li, J., He, T., Chekroud, A., Yeo, B., and Holmes, A. (2020). Convergent molecular, cellular, and cortical neuroimaging signatures of major depressive disorder. Proc Natl Acad Sci U S A *117*, 25138-25149.

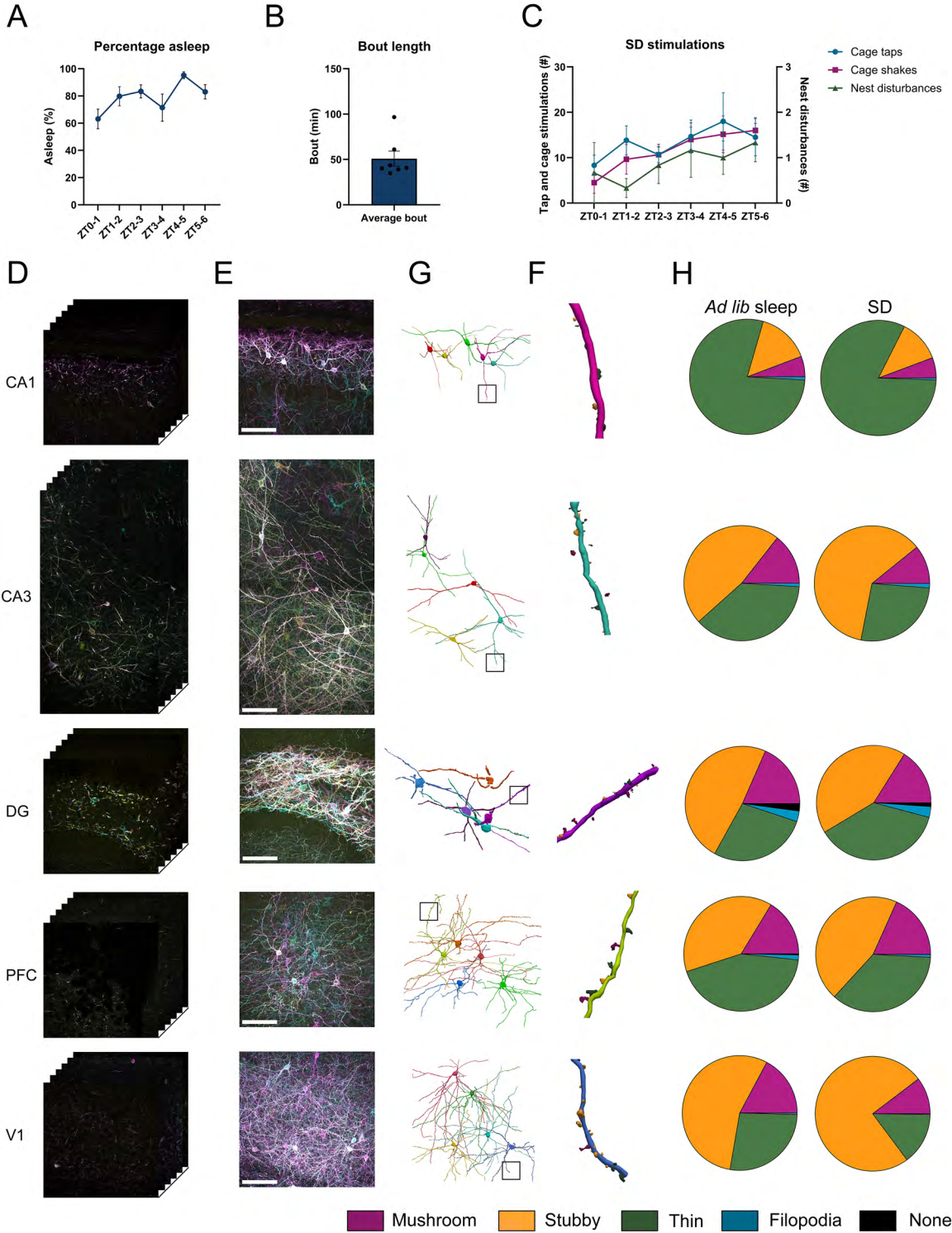
A
Percentage asleep
Asleep (%)
100
80
60
40
20
0
ZT0-1
ZT1-2
ZT2-3
ZT3-4
ZT4-5
ZT5-6
B
Bout length
Bout (min)
150
100
50
0
Average bout
C
SD stimulations
Tap and cage stimulations (#)
30
20
10
0
Nest disturbances (#)
3
2
1
0
ZT0-1 ZT1-2 ZT2-3 ZT3-4 ZT4-5 ZT5-6
Cage taps
Cage shakes
Nest disturbances
D
E
G
F
H
Ad lib sleep
SD
CA1
CA3
DG
PFC
V1
Mushroom
Stubby
Thin
Filopodia
None

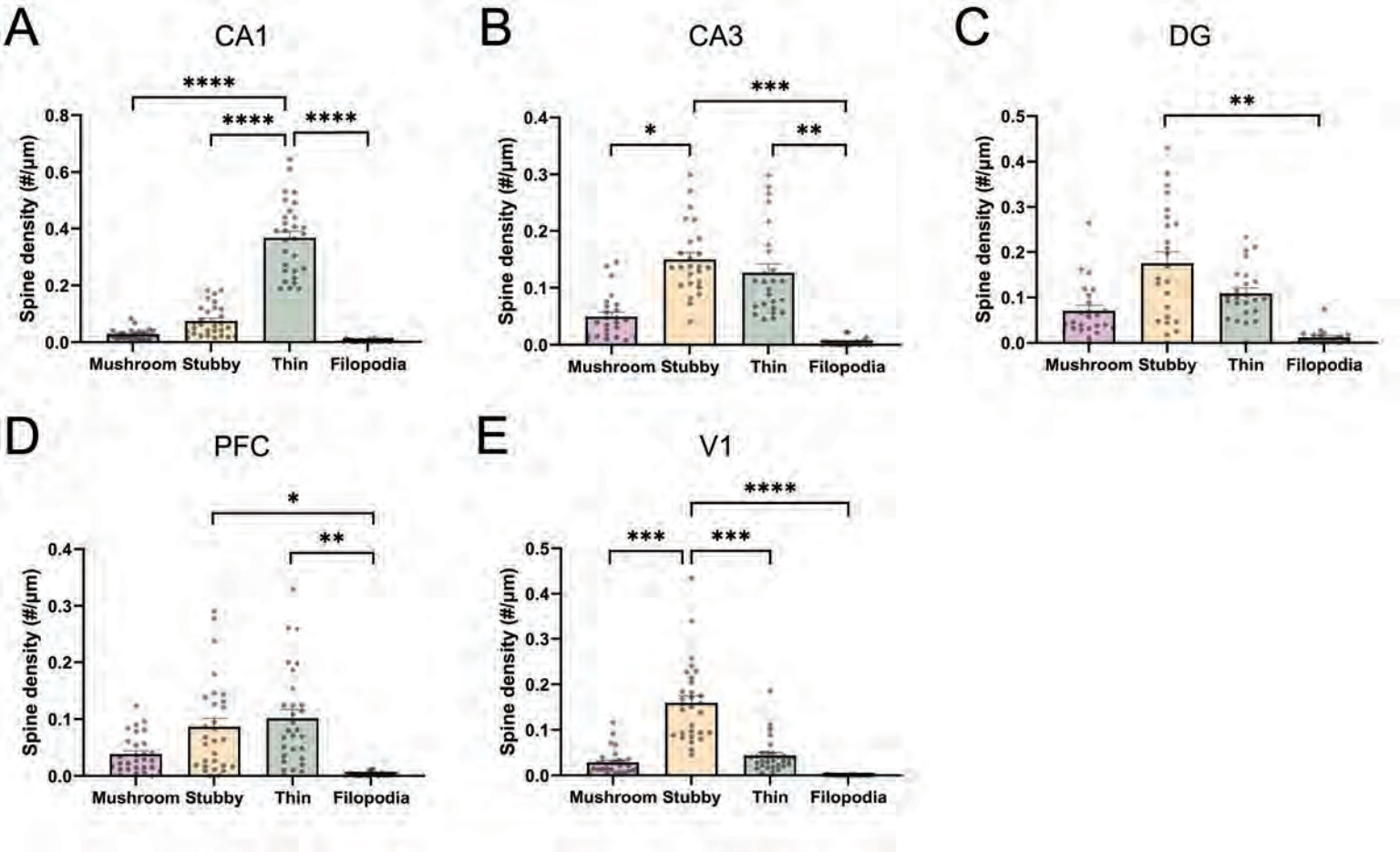
A
CA1
****
****
****
Spine density (#/µm)
0.0
0.2
0.4
0.6
0.8
Mushroom
Stubby
Thin
Filopodia
B
CA3
***
*
**
Spine density (#/µm)
0.0
0.1
0.2
0.3
0.4
Mushroom
Stubby
Thin
Filopodia
C
DG
**
Spine density (#/µm)
0.0
0.1
0.2
0.3
0.4
0.5
Mushroom
Stubby
Thin
Filopodia
D
PFC
*
**
Spine density (#/µm)
0.0
0.1
0.2
0.3
0.4
Mushroom
Stubby
Thin
Filopodia
E
V1
****
***
***
Spine density (#/µm)
0.0
0.1
0.2
0.3
0.4
0.5
Mushroom
Stubby
Thin
Filopodia

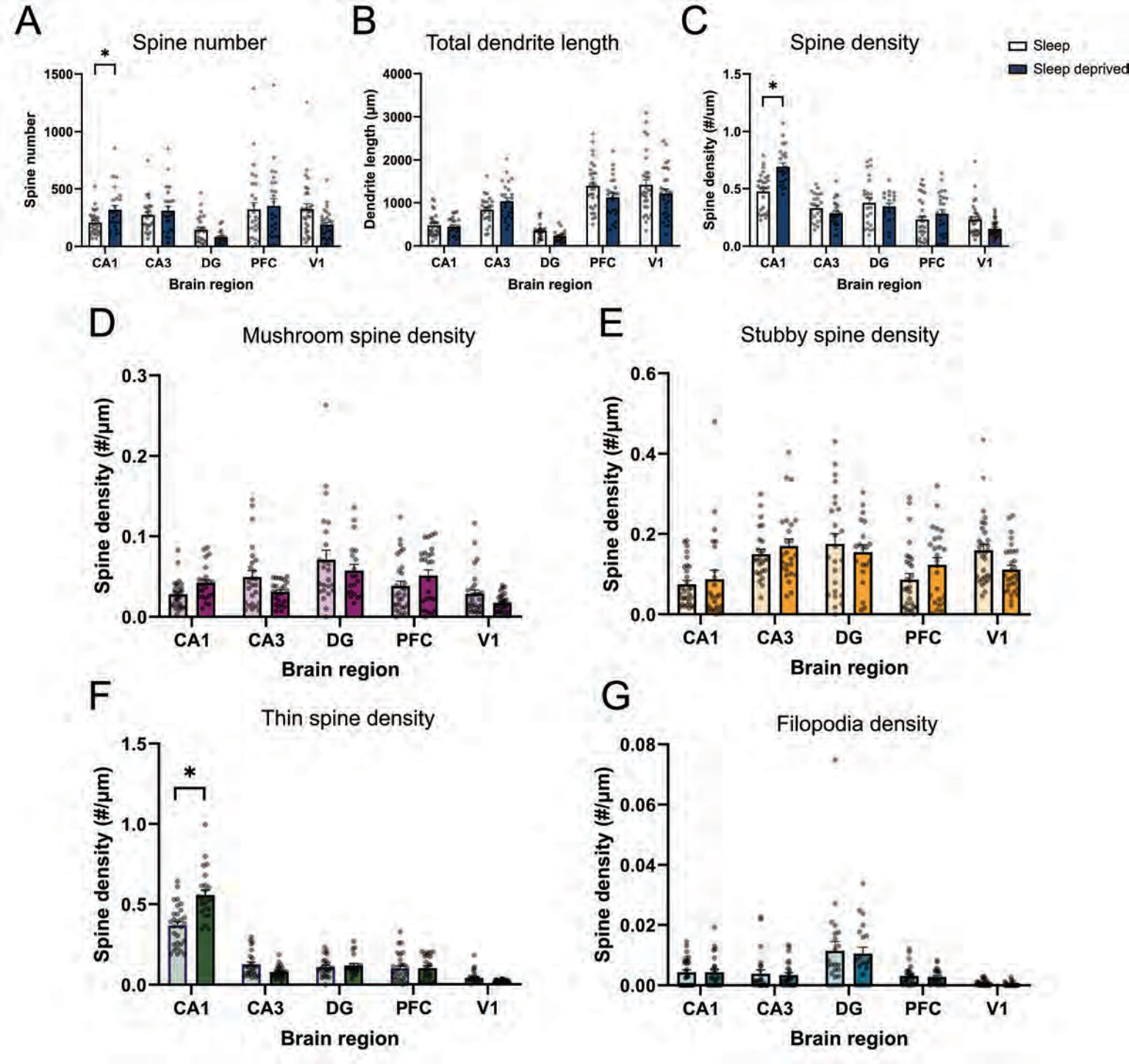
A
Spine number
Spine number
1500
1000
500
0
*
CA1
CA3
DG
PFC
V1
Brain region
B
Total dendrite length
Dendrite length (µm)
4000
3000
2000
1000
0
CA1
CA3
DG
PFC
V1
Brain region
C
Spine density
Sleep
Sleep deprived
Spine density (#/um)
1.5
1.0
0.5
0.0
*
CA1
CA3
DG
PFC
V1
Brain region
D
Mushroom spine density
Spine density (#/µm)
0.3
0.2
0.1
0.0
CA1
CA3
DG
PFC
V1
Brain region
E
Stubby spine density
Spine density (#/µm)
0.6
0.4
0.2
0.0
CA1
CA3
DG
PFC
V1
Brain region
F
Thin spine density
Spine density (#/µm)
1.5
1.0
0.5
0.0
*
CA1
CA3
DG
PFC
V1
Brain region
G
Filopodia density
Spine density (#/µm)
0.08
0.06
0.04
0.02
0.00
CA1
CA3
DG
PFC
V1
Brain region

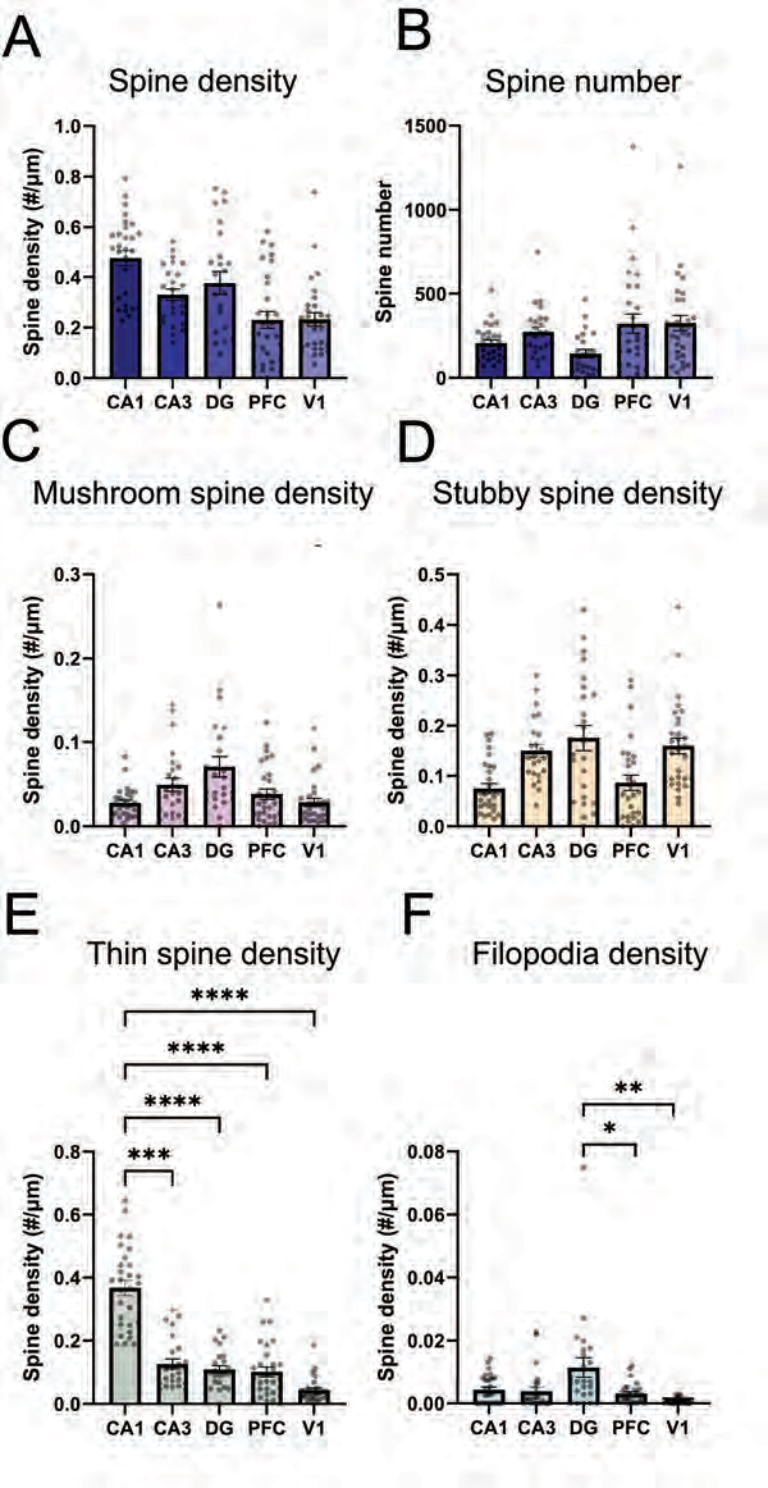
A
Spine density
Spine density (#/µm)
1.0
0.8
0.6
0.4
0.2
0.0
CA1 CA3 DG PFC V1
B
Spine number
Spine number
1500
1000
500
0
CA1 CA3 DG PFC V1
C
Mushroom spine density
Spine density (#/µm)
0.3
0.2
0.1
0.0
CA1 CA3 DG PFC V1
D
Stubby spine density
Spine density (#/µm)
0.5
0.4
0.3
0.2
0.1
0.0
CA1 CA3 DG PFC V1
E
Thin spine density
****
****
****
***
Spine density (#/µm)
0.8
0.6
0.4
0.2
0.0
CA1 CA3 DG PFC V1
F
Filopodia density
**
*
Spine density (#/µm)
0.08
0.06
0.04
0.02
0.00
CA1 CA3 DG PFC V1

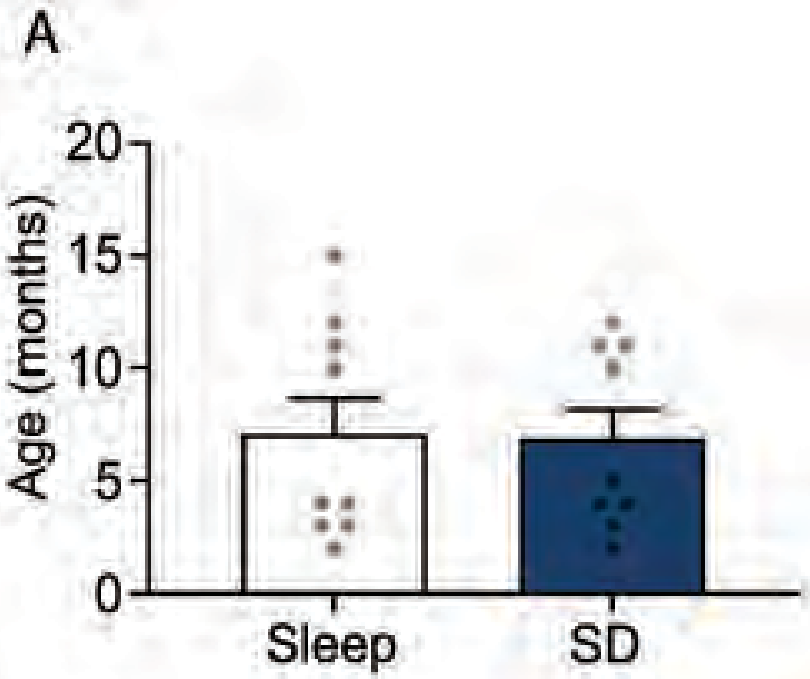
A
Age (months)
20
15
10
5
0
Sleep
SD

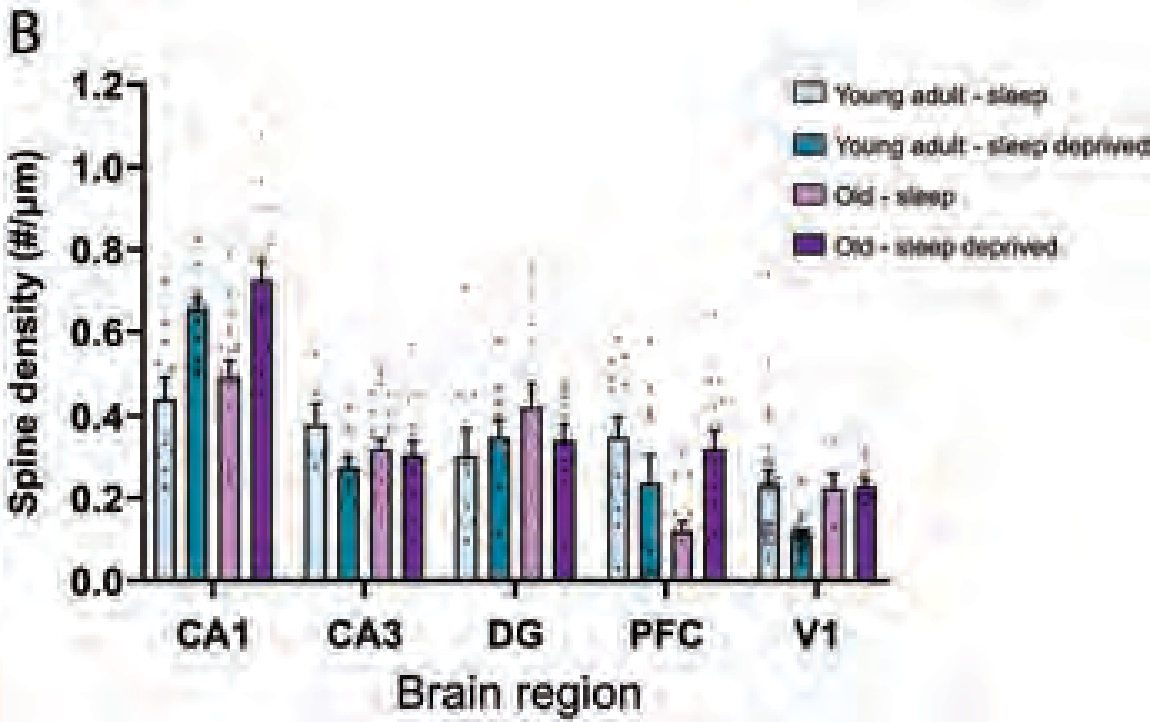
B
Spine density (#/µm)
1.2
1.0
0.8
0.6
0.4
0.2
0.0
Young adult - sleep
Young adult - sleep deprived
Old - sleep
Old - sleep deprived
CA1
CA3
DG
PFC
V1
Brain region

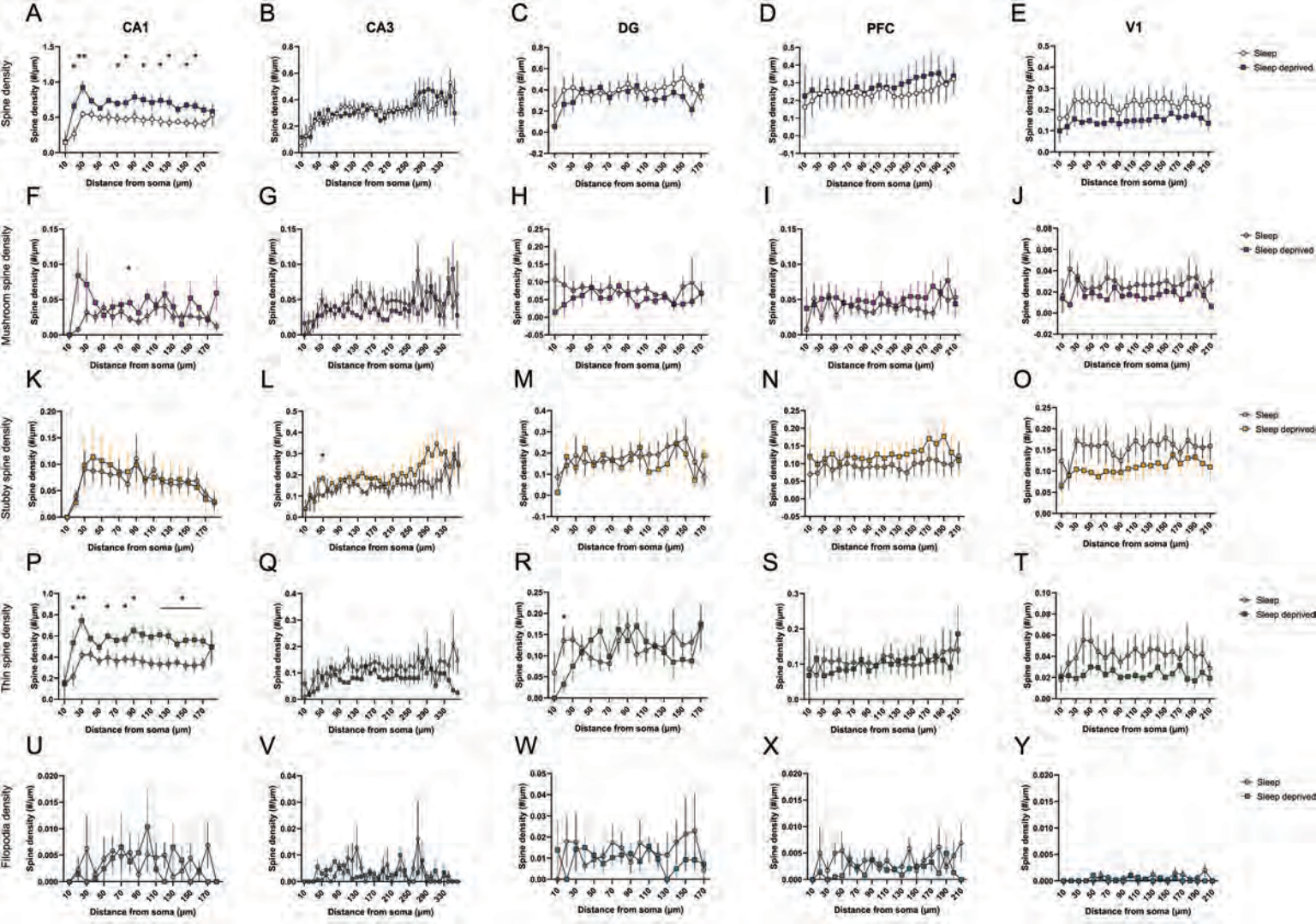
A
CA1
B
CA3
C
DG
D
PFC
E
V1
Spine density
Mushroom spine density
Stubby spine density
Thin spine density
Filopodia density
Spine density (#/µm)
Distance from soma (µm)
Sleep
Sleep deprived
F
G
H
I
J
K
L
M
N
O
P
Q
R
S
T
U
V
W
X
Y

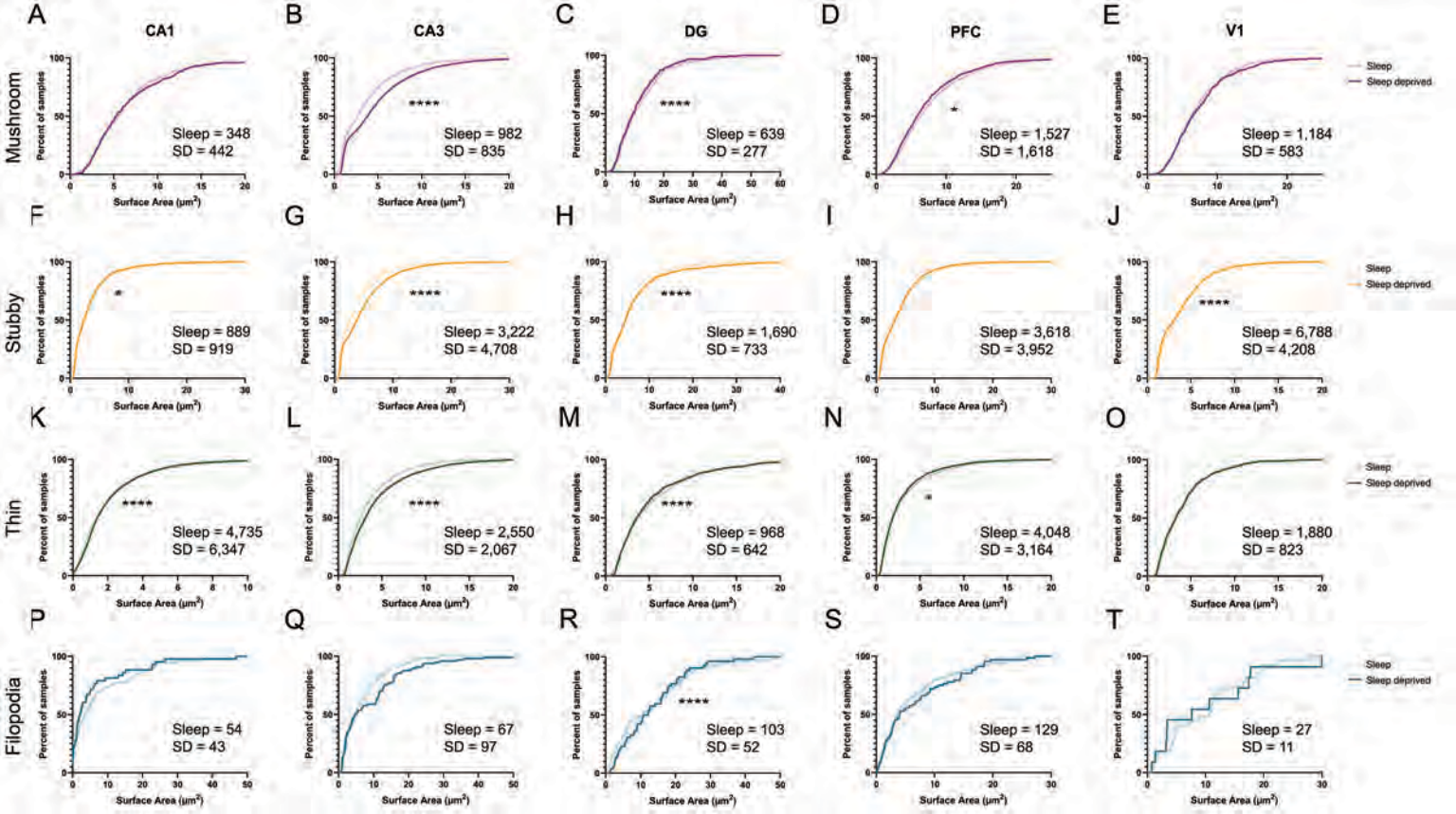
A
CA1
B
CA3
C
DG
D
PFC
E
V1
Mushroom
Sleep = 348
SD = 442
Sleep = 982
SD = 835
Sleep = 639
SD = 277
Sleep = 1,527
SD = 1,618
Sleep = 1,184
SD = 583
F
G
H
I
J
Stubby
Sleep = 889
SD = 919
Sleep = 3,222
SD = 4,708
Sleep = 1,690
SD = 733
Sleep = 3,618
SD = 3,952
Sleep = 6,788
SD = 4,208
K
L
M
N
O
Thin
Sleep = 4,735
SD = 6,347
Sleep = 2,550
SD = 2,067
Sleep = 968
SD = 642
Sleep = 4,048
SD = 3,164
Sleep = 1,880
SD = 823
P
Q
R
S
T
Filopodia
Sleep = 54
SD = 43
Sleep = 67
SD = 97
Sleep = 103
SD = 52
Sleep = 129
SD = 68
Sleep = 27
SD = 11
Percent of samples
Surface Area (μm²)
Sleep
Sleep deprived

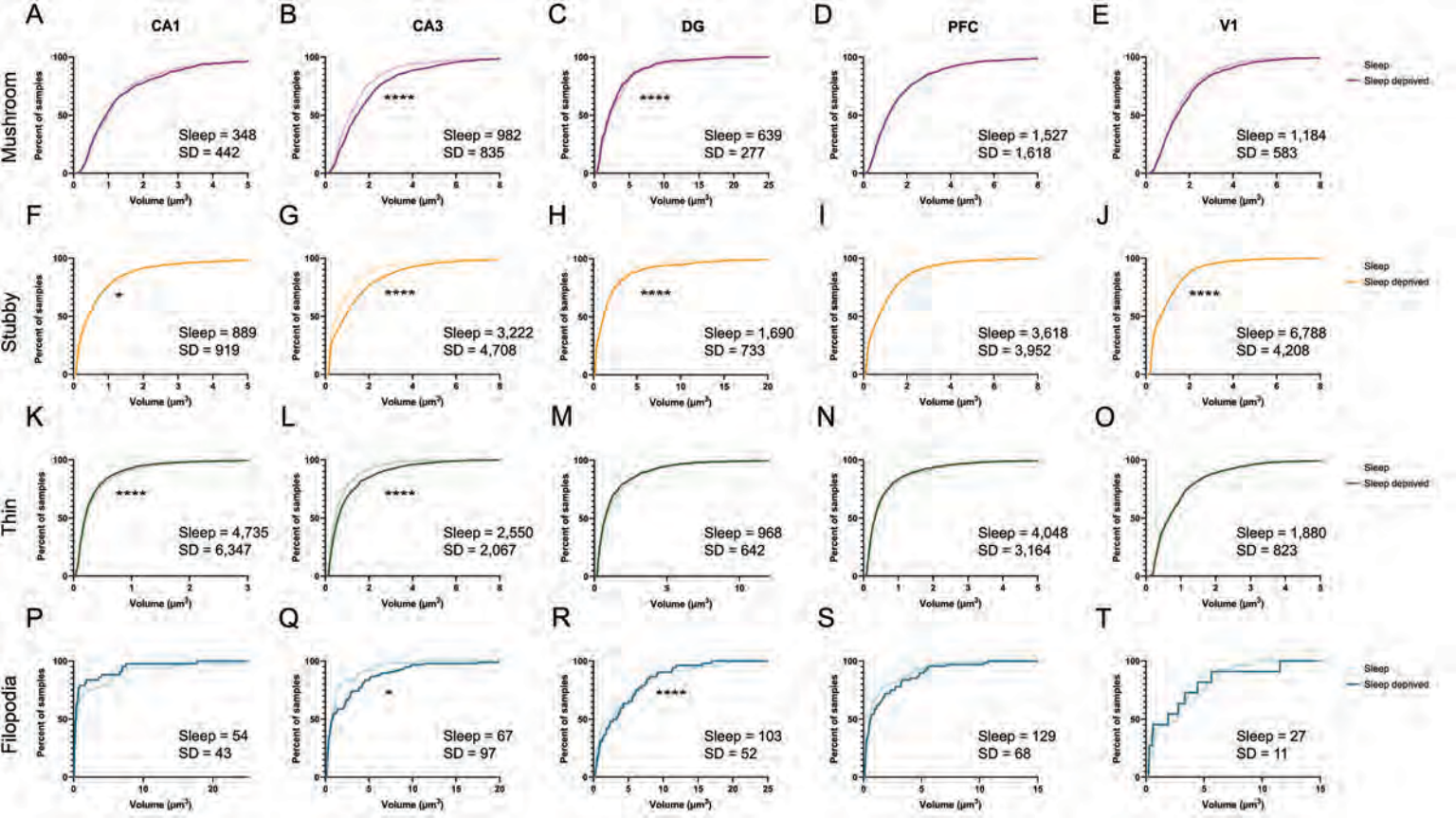
A
CA1
B
CA3
C
DG
D
PFC
E
V1
Mushroom
Sleep = 348
SD = 442
Sleep = 982
SD = 835
Sleep = 639
SD = 277
Sleep = 1,527
SD = 1,618
Sleep = 1,184
SD = 583
F
G
H
I
J
Stubby
Sleep = 889
SD = 919
Sleep = 3,222
SD = 4,708
Sleep = 1,690
SD = 733
Sleep = 3,618
SD = 3,952
Sleep = 6,788
SD = 4,208
K
L
M
N
O
Thin
Sleep = 4,735
SD = 6,347
Sleep = 2,550
SD = 2,067
Sleep = 968
SD = 642
Sleep = 4,048
SD = 3,164
Sleep = 1,880
SD = 823
P
Q
R
S
T
Filopodia
Sleep = 54
SD = 43
Sleep = 67
SD = 97
Sleep = 103
SD = 52
Sleep = 129
SD = 68
Sleep = 27
SD = 11
Percent of samples
Volume (μm³)
Sleep
Sleep deprived

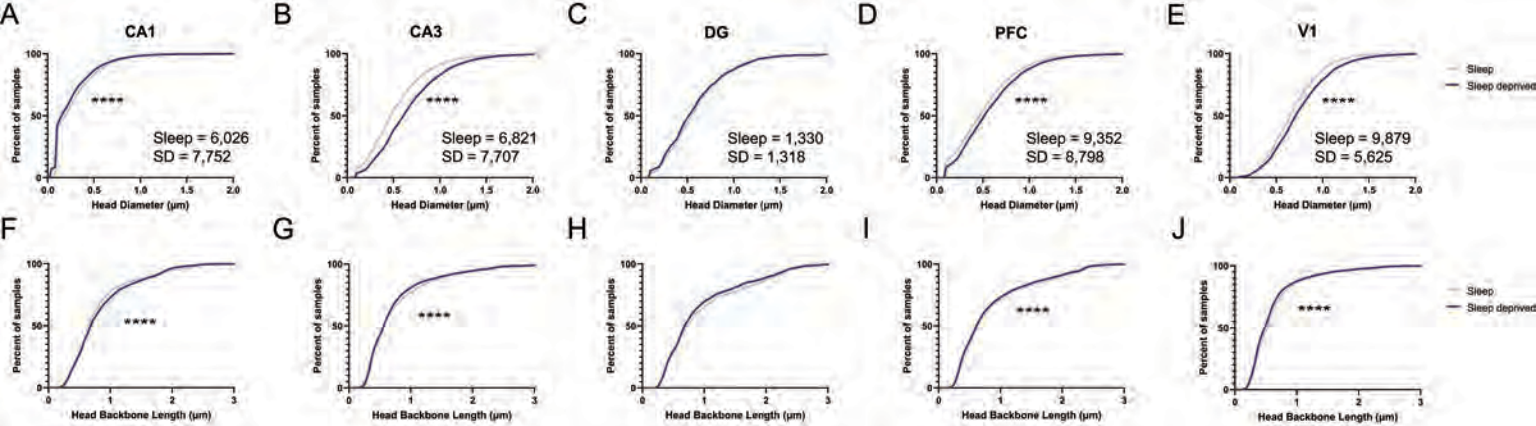
A
CA1
Sleep = 6,026
SD = 7,752
B
CA3
Sleep = 6,821
SD = 7,707
C
DG
Sleep = 1,330
SD = 1,318
D
PFC
Sleep = 9,352
SD = 8,798
E
V1
Sleep = 9,879
SD = 5,625
Sleep
Sleep deprived
Percent of samples
Head Diameter (µm)
Head Backbone Length (µm)
****
F
G
H
I
J

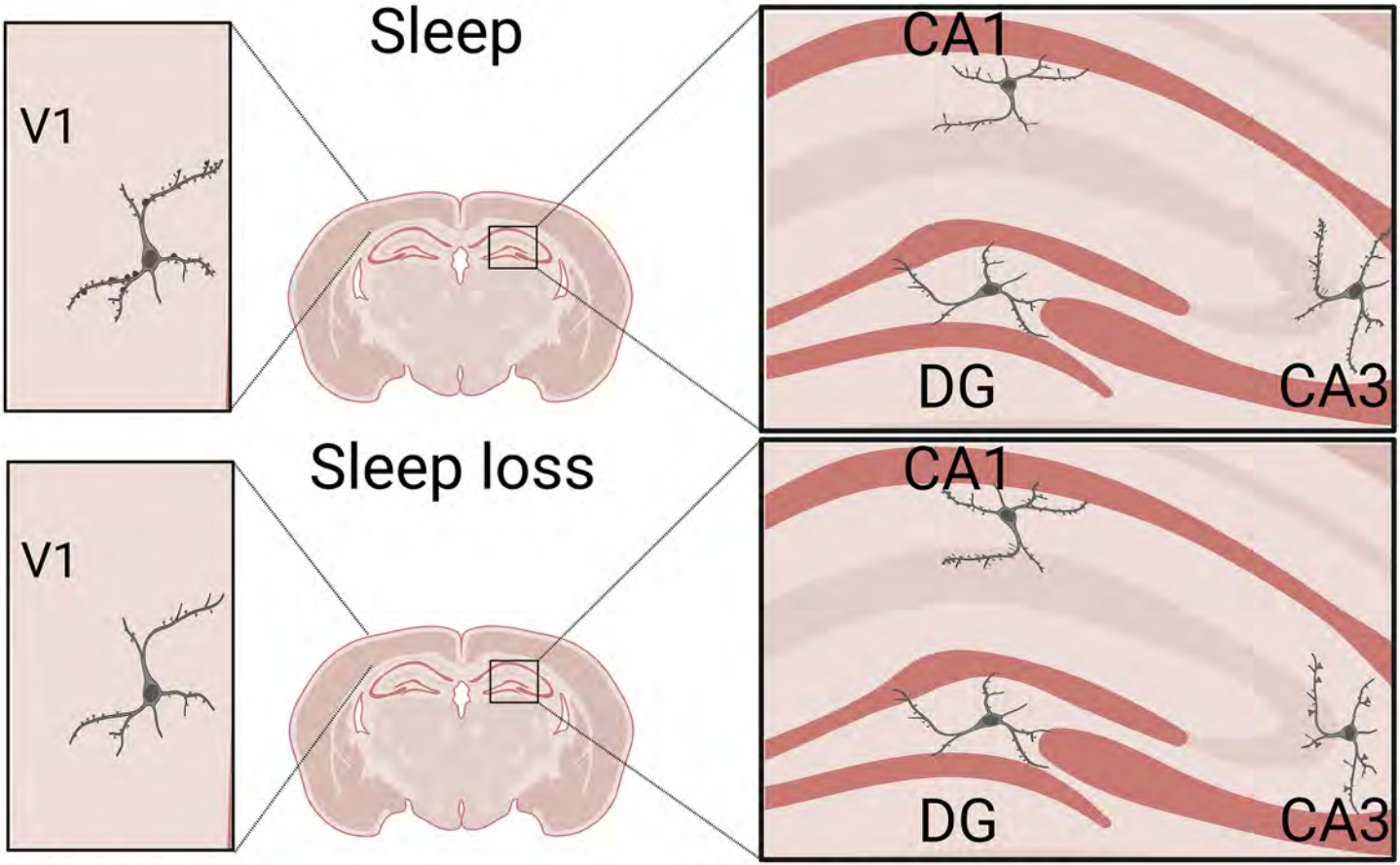

V1 ↓ stubby spine size

CA1 ↑ Thin spine density, ↓ size

CA3 ↑ size

DG - no change